GENERATIVE MODELING OF REGULAR AND IRREGULAR TIME SERIES DATA VIA KOOPMAN VAES

Ilan Naiman
Ben-Gurion University, UC Berkeley
`naimani@post.bgu.ac.il`

N. Benjamin Erichson
LBNL and ICSI
`erichson@lbl.gov`

Pu Ren
LBNL
`pren@lbl.gov`

Michael W. Mahoney
ICSI, LBNL, and UC Berkeley
`mmahoney@stat.berkeley.edu`

Omri Azencot
Ben-Gurion University
`azencot@cs.bgu.ac.il`

ABSTRACT

Generating realistic time series data is important for many engineering and scientific applications. Existing work tackles this problem using generative adversarial networks (GANs). However, GANs are unstable during training, and they can suffer from mode collapse. While variational autoencoders (VAEs) are known to be more robust to the these issues, they are (surprisingly) less considered for time series generation. In this work, we introduce Koopman VAE (KoVAE), a new generative framework that is based on a novel design for the model prior, and that can be optimized for either regular and irregular training data. Inspired by Koopman theory, we represent the latent conditional prior dynamics using a linear map. Our approach enhances generative modeling with two desired features: (i) incorporating domain knowledge can be achieved by leveraging spectral tools that prescribe constraints on the eigenvalues of the linear map; and (ii) studying the qualitative behavior and stability of the system can be performed using tools from dynamical systems theory. Our results show that KoVAE outperforms state-of-the-art GAN and VAE methods across several challenging synthetic and real-world time series generation benchmarks. Whether trained on regular or irregular data, KoVAE generates time series that improve both discriminative and predictive metrics. We also present visual evidence suggesting that KoVAE learns probability density functions that better approximate the empirical ground truth distribution.

1 INTRODUCTION

Generative modeling is an important problem in modern machine learning (Kingma & Welling, 2014; Goodfellow et al., 2014; Sohl-Dickstein et al., 2015), with a recent surge in interest due to results in natural language processing (Brown et al., 2020) and computer vision (Rombach et al., 2022; Ramesh et al., 2022). While image and text data have benefited from the recent development of generative models, time series (TS) data has received relatively little attention. This is in spite of the importance of generating TS data in various scientific and engineering domains, including seismology, climate studies, and energy analysis. Since these fields can face challenges in collecting sufficient data, e.g., due to high computational costs or limited sensor availability, high-quality generative models could be invaluable. However, generating TS data presents its own unique set of challenges. First, synthetic TS must preserve the related statistical distribution to fit into downstream forecasting, uncertainty quantification, and classification tasks. Second, advanced objectives such as supporting irregular sampling and integrating domain knowledge require models that respect the underlying dynamics (Che et al., 2018; Kidger et al., 2020; Jeon et al., 2022; Coletta et al., 2023).

Several existing state-of-the-art (SOTA) generative TS models are based on generative adversarial networks (GAN). For example, TimeGAN (Yoon et al., 2019) learns an embedding space where adversarial and supervised losses are optimized to mimic the data dynamics. Unfortunately, GANs are unstable during training and are prone to mode collapse, where the learned distribution is not sufficiently expressive (Goodfellow, 2016; Lucic et al., 2018; Saxena & Cao, 2021). In addition,

train sets with missing values or more generally, non-equispaced (irregularly-sampled) train sets, may be not straightforward to support in GAN architectures. For instance, Jeon et al. (2022) combine multiple different technologies to handle irregularly-sampled data, resulting in a complex system with many hyper-parameters. These challenges suggest that other generative paradigms should be also considered for generating time series information.

Surprisingly, variational autoencoders (VAEs) are not considered as strong baselines in generative time series benchmarks (Ang et al., 2023), although they suffer less from unstable training and mode collapse. In VAE, an approximate posterior is learned via a neural network to match a certain prior distribution that spans the data statistics. Recent methods including TimeVAE (Desai et al., 2021) and CR-VAE (Li et al., 2023) employ a variational viewpoint, however, their prior modeling is based on non-sequential standard normal priors. Thus, the learned posterior may struggle to properly represent the latent dynamics (Girin et al., 2021). This issue is further exacerbated when designing advanced sequential objectives. For instance, it is unclear how to incorporate domain knowledge about dynamical systems (e.g., stable dynamics, slow or fast converging or diverging dynamics) with unstructured Gaussian prior distributions. One promising direction to modeling latent dynamics is via *linear* approaches, that recently have been shown to improve performance and analysis (Zeng et al., 2023; Orvieto et al., 2023). More generally, this line of work aligns with theoretical and numerical tools from Koopman literature (Koopman, 1931; Rowley et al., 2009; Takeishi et al., 2017). Koopman theory offers a dual representation for autonomous dynamical systems via linear, albeit infinite-dimensional, operators. Harnessing this viewpoint facilitates autoencoder design, yielding finite-dimensional approximate Koopman operators that model the latent dynamics.

In this work, we propose Koopman VAE (KoVAE), a novel model that leverages linear latent Koopman dynamics within a VAE setup. KoVAE employs a prior stating that sequential latent data is governed by a *linear* dynamical system. Namely, the conditional prior distribution of the next latent variable, given the current variable, can be represented using a linear map. Under this assumption, we train an approximate posterior distribution that learns a nonlinear coordinate transformation of the inputs to a linear latent representation. Our approach offers two benefits: (i) it models the underlying dynamics and it respects the sequential nature of input data; and (ii) it seamlessly allows one to incorporate domain knowledge and study the qualitative behavior of the system by using spectral tools from dynamical systems theory. Moreover, we integrate into KoVAE a time-continuous module based on neural controlled differential equations (NCDE) (Kidger et al., 2020) to support irregularly-sampled time series information during training. The advantages of KoVAE are paramount as they facilitate the capturing of statistical and physical features of sequential information, and, in addition, imposing physics-constraints and analyzing the dynamics is straightforward.

Contributions. The main contributions of our work can be summarized as follows:

- We propose a new variational generative TS framework for regular and irregular data that is based on a **novel prior distribution** assuming an implicit linear latent Koopman representation. Our design and modeling yield a flexible, easy-to-code, and powerful generative TS model.

- We show that our approach facilitates **high-level capabilities** such as physics-constrained TS generation, by penalizing the eigenvalues of the approximated Koopman operator. We also perform stability analysis by inspecting the spectrum and its spread.

- We show improved state-of-the-art results in regular and irregular settings on several synthetic and real-world datasets, often surpassing strong baselines such as TimeGAN and GT-GAN by large margins. For instance, on the regular and irregular discriminative task we report a total mean relative improvement of **58%** and **49%** with respect to the second best approach, respectively.

2 RELATED WORK

Our work is related to generative models for TS as well as Koopman-based methods. Both areas enjoy increased interest in recent years, and thus, we focus our discussion on the most related work.

Generative Models for Time Series. Recurrent neural networks (RNNs) and their step-wise predictions have been used to generate sequences in Teacher forcing (Graves, 2013) and Professor forcing (Goyal et al., 2016) approaches. Autoregressive methods such as WaveNet (van den Oord et al., 2016) represent the predictive distribution of each audio sample by probabilistic conditioning on all previous samples, whereas TimeGCI (Jarrett et al., 2021) also incorporates GANs and optimizes a

transition policy where the reinforcement signal is provided by a global energy framework trained with contrastive estimation. Flow-based models for generating time series information utilize normalizing flows for an explicit likelihood distribution (Alaa et al., 2020). Long-range sequences were recently treated via state-space models (Zhou et al., 2023).

GANs and VAEs. GAN-based architectures have been shown to be effective for generating TS data. C-RNN-GAN (Mogren, 2016) directly applied GAN to sequential data, using LSTM networks for the generator and the discriminator. Recurrent Conditional GAN (Esteban et al., 2017) extends the latter work by dropping the dependence on the previous output while conditioning on additional inputs. TimeGAN (Yoon et al., 2019) is still one of the SOTA methods, and it jointly optimizes unsupervised and supervised loss terms to preserve the temporal dynamics of the training data during the generation process. COT-GAN (Xu et al., 2020) exploits optimal transport and temporal causal constraints to devise a new adversarial loss. Recently, GT-GAN (Jeon et al., 2022) was proposed as one of the few approaches that support irregular sampling, and it employs autoencoders, GANs, and Neural ODEs (Chen et al., 2018). While GAN techniques are more common in generative TS, there are also a few VAE-based approaches. A variational RNN was proposed in (Chung et al., 2015). TimeVAE (Desai et al., 2021) models the whole sequence by a global random variable with a normal Gaussian distribution for a prior, and they introduce trend and seasonality building blocks into the decoder. CR-VAE (Li et al., 2023) learns a Granger causal graph by predicting future data from past observations and using a multi-head decoder acting separately on latent variable coordinates. Additional related VAE works include (Rubanova et al., 2019; Li et al., 2020; Zhu et al., 2023).

Koopman-based Approaches. Koopman techniques have gained increasing interest over the past two decades, with applications ranging across analysis (Rowley et al., 2009; Schmid, 2010; Takeishi et al., 2017; Lusch et al., 2018; Azencot et al., 2019), optimization (Dogra & Redman, 2020; Redman et al., 2022), forecasting (Erichson et al., 2019; Azencot et al., 2020; Wang et al., 2023; Tayal et al., 2023), and disentanglement (Berman et al., 2023), among many others (Budišić et al., 2012; Brunton et al., 2021). Most related to our work are Koopman-based *probabilistic* models, which have received less attention in the literature. Deep variational Koopman models were introduced in Morton et al. (2019), allowing to sample from distributions over latent observables for prediction tasks. In Srinivasan & Takeishi (2020), the authors sample via Markov Chain Monte Carlo tools over transfer operators. A mean-field variational inference method with guaranteed stability was suggested in Pan & Duraisamy (2020) for the analysis and prediction of nonlinear dynamics. Finally, Han et al. (2022) designed a stochastic Koopman neural network for control that models the latent observables via a Gaussian distribution. To the best of our knowledge, our work is the first to combine VAEs and Koopman-based methods for generating regular and irregular TS information.

3 BACKGROUND

Below, we discuss background information essential to our method. In App. A and App. B, we also cover VAE and NCDE, used in our work to support irregularly-sampled sequential train sets.

Koopman theory and practice. The underlying theoretical justification for our work is related to dynamical systems and Koopman theory (Koopman, 1931). Let $\mathcal{M} \subset \mathbb{R}^m$ be a finite-dimensional domain and $\varphi : \mathcal{M} \to \mathcal{M}$ be a dynamical system defined by

$$x_{t+1} = \varphi(x_t) \,,$$

where $x_t \in \mathcal{M}$, and $t \in \mathbb{N}$ is a discrete variable that represents time. Remarkably, under some mild conditions (Eisner et al., 2015), there exists an infinite-dimensional operator known as the *Koopman operator* $\mathcal{K}_\varphi$ that acts on observable functions $f : \mathcal{M} \to \mathbb{C} \subset \mathcal{F}$ and it fully characterizes the dynamics. The operator $\mathcal{K}_\varphi$ is given by

$$\mathcal{K}_\varphi f(x_t) = f \circ \varphi(x_t) \,,$$

where $f \circ \varphi$ denotes composition of transformations. It can be shown that $\mathcal{K}_\varphi$ is linear, while φ may be nonlinear. Further, if the eigendecomposition of the Koopman operator exists, the eigenvalues and eigenvectors bear dynamical semantics. Spectral analysis of Koopman operators is currently still being researched (Mezić, 2013; Arbabi & Mezic, 2017; Mezic, 2017; Das & Giannakis, 2019). For instance, eigenfunctions whose eigenvalues lie within the unit circle are related to global stability (Mauroy & Mezić, 2016), and to orbits of the system (Mauroy & Mezić, 2013; Azencot et al.,
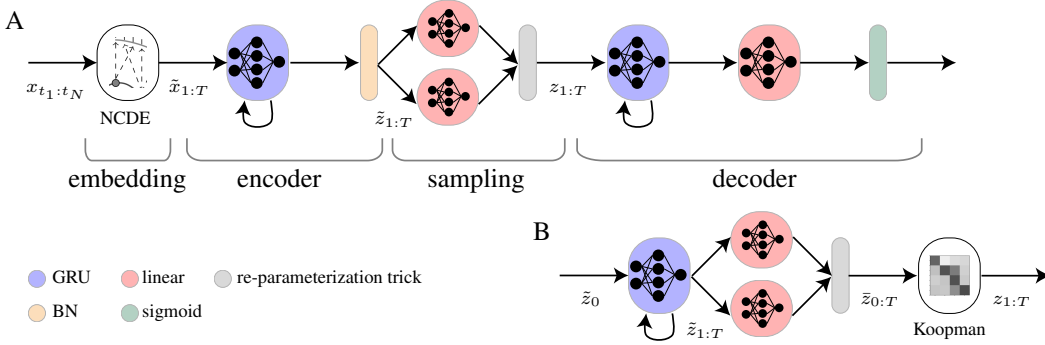
Figure 1: A) The posterior is composed of an embedding layer (NCDE), an encoder (GRU + BN), mean/variance computation and sampling (linear + repr. trick), and a decoder (GRU + linear + sigmoid). B) The prior consists of GRU, linear, a repr. trick layer, and our novel Koopman module.

2013; 2014). In practice, several methods have been devised to approximate the Koopman operator, of which, the dynamic mode decomposition (DMD) (Schmid, 2010) is perhaps the most well-known technique (Rowley et al., 2009). In this context, our work employs a learnable module akin to DMD in the model prior of our KoVAE as detailed below. In general, our approach can be viewed as treating the input data as states $x_{1:T}$, whereas the learnable linear dynamics we compute in KoVAE are parametrized by the latent observable functional space $\mathcal{F}$.

Sequential VAEs. We denote by $x_{1:T}$ a TS input $x_{1:T} = x_1, \ldots, x_T$, where $x_t \in \mathbb{R}^d$ for all t. Below, we focus on a general approach (Girin et al., 2021), where the joint distribution is given by

$$p(x_{1:T}, z_{1:T}) = p(z_{1:T})p(x_{1:T}|z_{1:T}) = \prod_{t=1}^{T} p(z_t|z_{<t}) \cdot \prod_{t=1}^{T} p(x_t|z_t) , \qquad (1)$$

where z_t is the prior latent code associated with x_t, it depends on all past variables $z_{<t}$, and given z_t, one can recover x_t via a neural decoder $p(x_t|z_t)$. The approximate posterior is modeled by

$$q(z_{1:T}|x_{1:T}) = \prod_{t=1}^{T} q(z_t|z_{<t}, x_{\leq t}) , \qquad (2)$$

namely, z_t is the posterior latent code, it is generated using the learned encoder $q(z_t|z_{<t}, x_{\leq t})$, and the dynamic VAE loss is composed of reconstruction and regularization terms and it reads

$$\mathcal{L}_{\text{VAE}} = \mathbb{E}_{z_{1:T} \sim q}[\log p(x_{1:T}|z_{1:T})] - \text{KL}[q(z_{1:T}|x_{1:T}) \,\|\, p(z_{1:T})] . \qquad (3)$$

4 KOOPMAN VARIATIONAL AUTOENCODERS (KOVAE)

To describe our generative model, we detail its sequential posterior in Sec. 4.1, its novel linear Koopman-based prior in Sec. 4.2, and its support for incorporating domain knowledge in Sec. 4.3.

4.1 A VARIATIONAL SEQUENTIAL POSTERIOR

To realize Eq. 2, our approximate posterior (Fig. 1A) is composed of embedding, encoder, sampling, and decoder modules. Given the irregular TS $x_{t_1:t_N}$, an NCDE embedding layer extracts a regularly-sampled TS $\tilde{x}_{1:T}$, followed by an encoder module consisting of a gated recurrent unit (GRU) layer (Cho et al., 2014) and batch normalization (BN) layer that learn the dynamics and output the latent representation $\tilde{z}_{1:T}$. Then, two linear layers produce the posterior mean $\mu(\tilde{z}_t)$ and variance $\sigma^2(\tilde{z}_t)$ for every t, allowing to employ the re-parameterization trick to generate the posterior series $z_{1:T}$ via

$$z_t \sim \mathcal{N}(\mu(\tilde{z}_t), \sigma^2(\tilde{z}_t)) . \qquad (4)$$

We feed the sampled code to the decoder that includes another GRU, a linear layer, and a sigmoid activation function. Note that the embedding NCDE layer is not used in the regular setting, i.e., when the input TS $x_{1:T}$ is regularly sampled.

4.2 A NOVEL LINEAR VARIATIONAL SEQUENTIAL PRIOR

In general, one of the fundamental tasks in variational autoencoders' design and modeling is the choice of prior distribution. For instance, static VAEs define it to be a normal Gaussian distribution, i.e., $p(z) = \mathcal{N}(0, I)$, among other choices, e.g., (Huszár, 2017). In the sequential setting, a common choice for the prior is a sequence of Gaussians (Chung et al., 2015) given by

$$p(z_t | z_{<t}) = \mathcal{N}(\mu(z_{<t}; \theta), \sigma^2(z_{<t}; \theta)) , \tag{5}$$

where the mean and variance are learned with a NN, and $z_{1:T}$ represents the latent sequence. Now, the question arises whether one can model the prior of generative TS models $p(z_{1:T}) = \prod_{t=1}^{T} p(z_t | z_{<t})$ in Eq. 1 so that it associates better with the underlying dynamics. In what follows, we propose a novel inductive bias leading to a new VAE modeling paradigm.

Prior modeling. In this work, instead of considering a nonlinear sequence of Gaussian as in Eq. 5, we assume that there exists a learnable nonlinear coordinate transformation mapping inputs to a *linear* latent space. That is, the inputs $x_{t_1:t_N}$ are transformed to $z_{1:T}$ whose dynamics are governed by a linear sequence of Gaussians, see inset for an illustration. Formally, the forward propagation in time of z_t is governed by a matrix, i.e.,

$$z_t := \mathbb{E}_{A \sim \mathcal{A}} [A z_{t-1}] , \tag{6}$$

for every t, where $A \in \mathbb{R}^{k \times k}$ is sampled from a space of linear operators $\mathcal{A}$. In practice, we implement the prior (Fig. 1B) and produce $z_{1:T}$ using a gated recurrent unit (GRU) layer, a sampling component, and a Koopman module (Takeishi et al., 2017). Given $\tilde{z}_0 := \vec{0}$, the GRU yields $\tilde{z}_{1:T}$ that is fed to two linear layers which produce the mean $\mu(\tilde{z}_t)$ and variance $\sigma^2(\tilde{z}_t)$ for every t, allowing to sample $\bar{z}_t$ from $\tilde{z}_{1:T}$ via Eq. 5. To compute A, we construct two matrices $\bar{Z}_0, \bar{Z}$ with $\bar{z}_{0:T-1}$ and $\bar{z}_{1:T}$ in their columns, respectively, where $\bar{z}_0 \sim \mathcal{N}(\mu(0; \theta), \sigma^2(0; \theta))$. Then, we solve the linear system for the best A such that $A\bar{Z}_0 = \bar{Z}$, similar to DMD (Schmid, 2010). Finally, z_t is defined to be $z_t := A\bar{z}_{t-1}$.

Training objective. Effectively, it may be that A induces some error, i.e., $z_t \neq \bar{z}_t$ for some $t \in [1, \ldots, T]$. Thus, we introduce an additional predictive loss term that promotes linearity in the prior latent variables by matching between $\bar{z}_{1:T}$ and $z_{1:T}$, namely,

$$\mathcal{L}_{\text{pred}}(z_{1:T}, \bar{z}_{1:T}) = \mathbb{E}_{\bar{z}_{1:T} \sim p}[\log p(z_{1:T} | \bar{z}_{1:T})] . \tag{7}$$

Combining the penalties from Sec. 3 and the loss Eq. 7, we arrive at the following training objective which includes a reconstruction term, a prediction term, and a regularization term,

$$\mathcal{L} = \mathbb{E}_{z_{1:T} \sim q}[\log p(x_{t_1:t_N} | z_{1:T})] + \alpha \mathcal{L}_{\text{pred}}(z_{1:T}, \bar{z}_{1:T}) - \beta \text{KL}[q(z_{1:T} | x_{t_1:t_N}) \| p(z_{1:T})] , \tag{8}$$

where $\alpha, \beta \in \mathbb{R}^+$ are user weights, similar to (Higgins et al., 2016). In App. C, we provide technical details on $\mathcal{L}$, and in App. D, we show that our objective is a penalized evidence lower bound (ELBO).

4.3 PHYSICS-CONSTRAINED GENERATION AND ANALYSIS

The matrix A computed in Sec. 4.2 encodes the latent dynamics in a linear form. Thus, it can be constrained and evaluated using spectral tools from dynamical systems theory (Strogatz, 2018). For instance, the eigenvalues $\lambda_j \in \mathbb{C}, j = 1, \ldots, k$, are associated with growth ($|\lambda_j| > 1$) and decay ($|\lambda_j| < 1$), whereas the eigenvectors $\phi_j \in \mathbb{C}^k$ encode the dominant modes. Our constrained generation and interpretability results are based on the relation between A and dynamical systems.

Often, prior knowledge of the problem can be utilized in the generation of time series information, see e.g., the example in Sec. 5. Our framework allows us to directly incorporate such knowledge by constraining the eigenvalues of the system, as was recently proposed in (Berman et al., 2023). Specifically, we denote by $c_1, \ldots, c_r \subset \mathbb{C}$ with $r \leq k$ several known constant values, and we define the following penalty we add to the optimization that yields A whose eigenvalues are denoted by λ_j,

$$\mathcal{L}_{\text{eig}} = \sum_{j=1}^{r} ||\lambda_j| - c_j|^2 , \tag{9}$$

where $|\lambda_j|$ is the modulus of a complex number. The loss term 9 can be used during training or inference, or both. For instance, stable dynamical systems as we consider in Sec. 5.2, have Koopman operators with eigenvalues on the unit circle, i.e., $|\lambda_j| = 1$. Thus, when constraining the dynamics, we can fix some $c_1, \ldots, c_r = 1$, and leave the rest to be unconstrained. In addition to constraining the spectrum, we can also analyze the spectrum to study the stability behavior of the system, similarly to (Erichson et al., 2019; Naiman & Azencot, 2023), see also Sec. 5.2.

5 EXPERIMENTS

In this section, we detail the results of our extensive experiments. Details related to datasets and baselines are provided in App. E. Our code is available at GitHub.

5.1 GENERATIVE TIME SERIES RESULTS

In what follows, we demonstrate our model's generation capabilities empirically, and we evaluate our method both quantitatively and qualitatively in the tests we describe below.

Quantitative evaluation. Yoon et al. (2019) suggested two tasks for evaluating generative time series models: the discriminative task and the predictive task. In the *discriminative test*, we measure the similarity between real and artificial samples. First, we generate a collection of artificial samples $\{y_{1:T}^j\}_{j=1}^N$ and we label them as 'fake'. Second, we train a classifier to discriminate between the fake and the real dataset $\{x_{1:T}^j\}_{j=1}^N$. Finally, we report the value $|\frac{1}{2} - \text{acc}|$, where acc is the accuracy of the discriminator on a held-out set. Thus, a lower discriminative score implies better generated data as it fools the discriminator. The *predictive task* is based on the "train on synthetic, test on real" protocol. We we train a predictor on the generated artificial samples. Then, the predictor is evaluated on the real data. A lower mean absolute error (MAE) indicates improved predictions.

We consider the discriminative and predictive tasks in two evaluation cases: *regular*, where we use the entire dataset; and *irregular*, where we omit a portion of the dataset. Specifically, in the irregular setting, we follow Jeon et al. (2022), and we randomly omit $30\%, 50\%$, and 70% of the observations. We show in Tab. 1 and Tab. 2 the discriminative and predictive scores, respectively. Tab. 1 lists at the bottom the relative improvement (RI) of the best score s_1 with respect to the second best score s_2, i.e., $|s_2 - s_1|/s_2$. Tab. 2 details the predictive scores obtained when the real data is used in the task (original). Both tables highlight the best scores. The results show that our approach (KoVAE) attains the best scores on both tasks. In particular, KoVAE demonstrates significant improvements on the discriminative tasks, yielding a remarkable average RI of **58%**. In Tab. 3, we detail the discriminative and predictive scores for the irregular setting. Similarly to the regular case, KoVAE presents the best measures, except for predictive Stocks 50% and discriminative Energy 70%. Still, our average RIs are significant: **48%, 55%**, and **43%** for the three different irregular settings.

Qualitative evaluation. Next, we use qualitative metrics to examine the similarity of the generated sequences to the real data. We consider two visualization techniques: (i) we project the real and

Table 1: Regular TS, discriminative task

Method	Sines	Stocks	Energy	MuJoCo
KoVAE (Ours)	**0.005**	**0.009**	**0.143**	**0.076**
GT-GAN	0.012	0.077	0.221	0.245
TimeVAE	0.016	0.036	0.323	0.224
TimeGAN	0.011	0.102	0.236	0.409
CR-VAE	0.342	0.320	0.475	0.464
RCGAN	0.022	0.196	0.336	0.436
C-RNN-GAN	0.229	0.399	0.499	0.412
T-Forcing	0.495	0.226	0.483	0.499
P-Forcing	0.430	0.257	0.412	0.500
WaveNet	0.158	0.232	0.397	0.385
WaveGAN	0.277	0.217	0.363	0.357
RI	**54.54%**	**75.00%**	**35.29%**	**66.07%**

Table 2: Regular TS, predictive task

Method	Sines	Stocks	Energy	MuJoCo
KoVAE (Ours)	**0.093**	**0.037**	**0.251**	**0.038**
GT-GAN	0.097	0.040	0.312	0.055
TimeVAE	**0.093**	0.037	0.254	0.039
TimeGAN	0.093	0.038	0.273	0.082
CR-VAE	0.143	0.076	0.277	0.050
RCGAN	0.097	0.040	0.292	0.081
C-RNN-GAN	0.127	0.038	0.483	0.055
T-Forcing	0.150	0.038	0.315	0.142
P-Forcing	0.116	0.043	0.303	0.102
WaveNet	0.117	0.042	0.311	0.333
WaveGAN	0.134	0.041	0.307	0.324
Original	0.094	0.036	0.250	0.031

Table 3: Irregular time series (30%, 50% and 70% of observations are dropped)

		30%				50%				70%			
		Sines	Stocks	Energy	MuJoCo	Sines	Stocks	Energy	MuJoCo	Sines	Stocks	Energy	MuJoCo
Discriminative Score	KoVAE (Ours)	**0.035**	**0.162**	**0.280**	**0.123**	**0.030**	**0.092**	**0.298**	**0.117**	**0.065**	**0.101**	0.392	**0.119**
	GT-GAN	0.363	0.251	0.333	0.249	0.372	0.265	0.317	0.270	0.278	0.230	**0.325**	0.275
	TimeGAN-$\triangle t$	0.494	0.463	0.448	0.471	0.496	0.487	0.479	0.483	0.500	0.488	0.496	0.494
	RCGAN-$\triangle t$	0.499	0.436	0.500	0.500	0.406	0.478	0.500	0.500	0.433	0.381	0.500	0.500
	C-RNN-GAN-$\triangle t$	0.500	0.500	0.500	0.500	0.500	0.500	0.500	0.500	0.500	0.500	0.500	0.500
	T-Forcing -$\triangle t$	0.395	0.305	0.477	0.348	0.408	0.308	0.478	0.486	0.374	0.365	0.468	0.428
	P-Forcing-$\triangle t$	0.344	0.341	0.500	0.493	0.428	0.388	0.498	0.491	0.288	0.317	0.500	0.498
	TimeGAN-D	0.496	0.411	0.479	0.463	0.500	0.477	0.473	0.500	0.498	0.485	0.500	0.492
	RCGAN-D	0.500	0.500	0.500	0.500	0.500	0.500	0.500	0.500	0.500	0.500	0.500	0.500
	C-RNN-GAN-D	0.500	0.500	0.500	0.500	0.500	0.500	0.500	0.500	0.500	0.500	0.500	0.500
	T-Forcing-D	0.408	0.409	0.347	0.494	0.430	0.407	0.376	0.498	0.436	0.404	0.336	0.493
	P-Forcing-D	0.500	0.480	0.491	0.500	0.499	0.500	0.500	0.500	0.500	0.449	0.494	0.499
Predictive Score	KoVAE (Ours)	**0.074**	**0.019**	**0.049**	**0.043**	**0.072**	0.019	**0.049**	**0.042**	**0.076**	**0.012**	**0.052**	**0.044**
	GT-GAN	0.099	0.021	0.066	0.048	0.101	**0.018**	0.064	0.056	0.088	0.020	0.076	0.051
	TimeGAN-$\triangle t$	0.145	0.087	0.375	0.118	0.123	0.058	0.501	0.402	0.734	0.072	0.496	0.442
	RCGAN-$\triangle t$	0.144	0.181	0.351	0.433	0.142	0.094	0.391	0.277	0.218	0.155	0.498	0.222
	C-RNN-GAN-$\triangle t$	0.754	0.091	0.500	0.447	0.741	0.089	0.500	0.448	0.751	0.084	0.500	0.448
	T-Forcing-$\triangle t$	0.116	0.070	0.251	0.056	0.379	0.075	0.251	0.069	0.113	0.070	0.251	0.053
	P-Forcing-$\triangle t$	0.102	0.083	0.255	0.089	0.120	0.067	0.263	0.189	0.123	0.050	0.285	0.117
	TimeGAN-D	0.192	0.105	0.248	0.098	0.169	0.254	0.339	0.375	0.752	0.228	0.443	0.372
	RCGAN-D	0.388	0.523	0.409	0.361	0.519	0.333	0.250	0.314	0.404	0.441	0.349	0.420
	C-RNN-GAN-D	0.664	0.345	0.440	0.457	0.754	0.273	0.438	0.479	0.632	0.281	0.436	0.479
	T-Forcing-D	0.100	0.027	0.090	0.100	0.104	0.038	0.090	0.113	0.102	0.031	0.091	0.114
	P-Forcing-D	0.154	0.079	0.147	0.173	0.190	0.089	0.198	0.207	0.278	0.107	0.193	0.191
	Original	0.071	0.011	0.045	0.041	0.071	0.011	0.045	0.041	0.071	0.011	0.045	0.041

synthetic data into a two-dimensional space using `t-SNE` (Van der Maaten & Hinton, 2008); and
(ii) we perform kernel density estimation by visualizing the probability density functions (PDF). In
Fig. 2, we visualize the synthetic and real two-dimensional point clouds in the irregular 50% setting
for all datasets via `t-SNE` (top row), and additionally, we visualize their corresponding probability
density functions (bottom row). Further, we also show the PDF of GT-GAN (Jeon et al., 2022) in
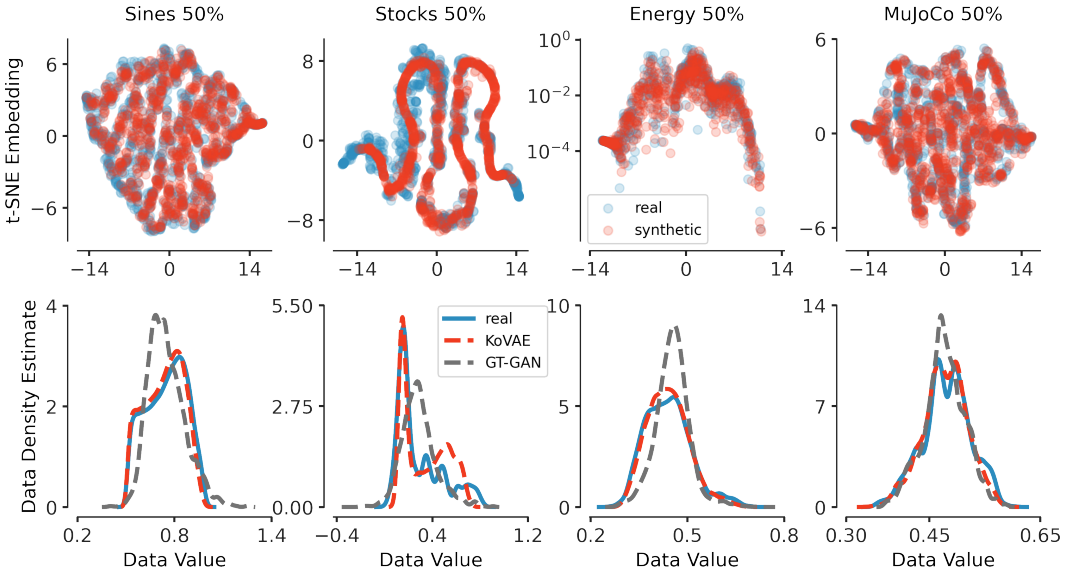dashed-black curves at the bottom row. Overall, our approach displays strong correspondences in

Figure 2: We qualitatively evaluate our approach with two-dimensional `t-SNE` plots of the synthetic
and real data (top row). In addition, we show the probability density functions of the real data, and
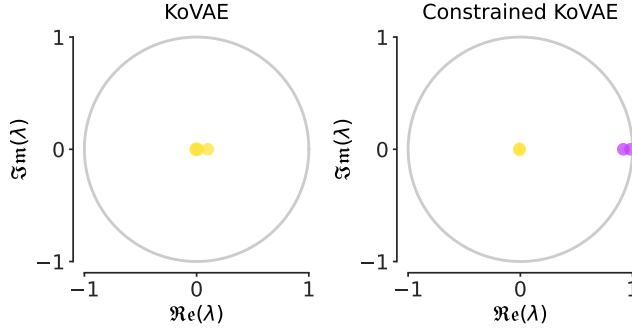for KoVAE and GT-GAN synthetic distributions (bottom row).

Figure 3: On the left, we show the spectrum of the approximate Koopman operator without constraints during the training. On the right, we show the spectrum of the approximate Koopman operator for the model that is trained with stability constraints. We can see that, indeed, the absolute value of two eigenvalues is approximately 1.

both visualizations, where in Fig. 2 (top row), we observe a high overlap between real and synthetic samples, and in Fig. 2 (bottom row), the PDFs show a similar trend and behavior. On Stocks 50%, we identify lower variability in KoVAE in comparison to the real data that present a larger variance. In App. H, we provide additional results for the regular and irregular 30%, and 70% cases.

5.2 Physics-Constrained Generation

In this section, we demonstrate how to incorporate prior knowledge of the problem when generating time series information. While we could study the Sines dataset, we opted for a more challenging test case, and thus, we focus on the *nonlinear pendulum* system. Let $l = 1$ and $g = 9.8$ denote the length and gravity, respectively. Then, we consider the following ordinary differential equation (ODE) that describes the evolution of the angular displacement from an equilibrium θ,

$$\frac{\mathrm{d}^2\,\theta}{\mathrm{d}\,t^2} + \frac{g}{l}\sin\theta = 0 \,, \quad \theta(0) = 0 \,, \quad \dot\theta(0) = 0 \,. \tag{10}$$

To generate N different sequences, we uniformly sample $\theta^j(0) \sim \mathcal{U}(0.5, 2.7)$ for $j = 1, \ldots, N$ over the time interval $t = [0, 17]$, where the time step is defined by $\Delta t = 0.1$. This results in a set $\{x_{1:T}^j\}_{j=1}^N$ with $T = 170$ and each time sample is two-dimensional, i.e., $x_t \in \mathbb{R}^2$. To simulate real-world noisy sensors, we incorporate additive Gaussian noise to each sample. Namely, we sample $\rho \sim \mathcal{N}(0, 1)$, and we define the train set samples via $\bar{x}_t := x_t + 0.08\,\rho$.

We evaluate the nonlinear pendulum on three different models: (i) a KoVAE with $\alpha = 0$; (ii) a KoVAE; and (iii) a KoVAE with an eigenvalue constraint as described in Sec. 4.3. Specifically, we train all models with a fixed latent size κ of z_t to be $\kappa = 4$. For the constrained version, we additionally add $\mathcal{L}_{\mathrm{eig}}$:

$$\mathcal{L}_{\mathrm{eig}} = ||\lambda_p| - c_p|^2 + ||\lambda_q| - c_q|^2 \,, \tag{11}$$

where $c_p = 1, c_q = 1$ and λ_p and λ_q are the largest eigenvalues during training. We define this constraint since the nonlinear pendulum is a stable dynamical system that is governed by *two* modes. The rest of the eigenvalues, λ_i, where $i \neq p, q$ could be additionally constrained to be equal to zero. However, we observe that when we leave the rest of the eigenvalues to be unconstrained, we get a similar behavior. Fig. 3 shows the spectra of the linear operators associated with KoVAE and ***constrained*** KoVAE. We can analyze and interpret the learned dynamics by investigating the spectrum. Specifically, if $|\lambda_j| < 1$, it is associated with exponentially decaying modes since $\lim_{t\to\infty} |\lambda_j^t| = 0$. When $|\lambda_j| = 1$, the associated mode has infinite memory, whereas $|\lambda_j| > 1$ is associated with unstable behavior of the dynamics since $\lim_{t\to\infty} |\lambda_j^t| = \infty$. In Fig. 3, we observe that training without the constraint results in decaying dynamics where all eigenvalues $\ll 1$ (yellow). In contrast, analyzing our approximate operator reveals that as expected, $|\lambda_p|$ and $|\lambda_q|$ (purple) are approximately one, indicating stable dynamics and the rest (yellow) are approximately zero, as desired. Finally, we also compute the spectra associated with the computed operators in the regular setting and discussed the results in App. F.
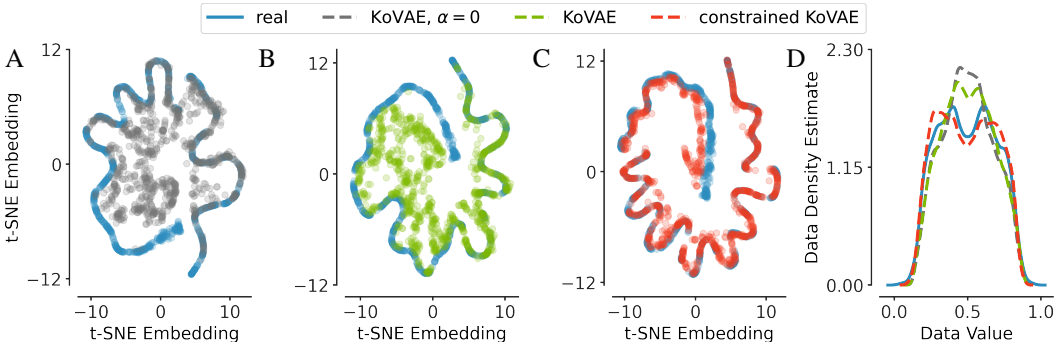
Figure 4: The t-SNE plots of KoVAE with $\alpha = 0$ (A), KoVAE (B), and constrained KoVAE (C), and their probability density functions (D) are compared to the true nonlinear pendulum data.

In addition to analyzing the spectrum, we visualize in Fig. 4 the t-SNE plots of the real data in comparison to the data generated using the three trained models, KoVAE with $\alpha = 0$ in Fig. 4A, KoVAE in Fig. 4B, and constrained KoVAE in Fig. 4C. Further, we also plot the probability density functions of the three models in Fig. 4D. The results clearly show that the synthetic samples generated with the constrained KoVAE (red) better match the distribution and PDF of the true process in comparison to KoVAE (green) and KoVAE with $\alpha = 0$ (gray).

5.3 ABLATION STUDY

We ablate our approach on the discriminative task in the regular and 30% and 50% irregular settings. We eliminate the linear prior by fixing $\alpha = 0$, and we also train another baseline without the linear prior and without the recurrent (GRU) component. Tab. 4 details our ablation results, and we observe that KoVAE outperforms all other regular ablation baselines and the majority of irregular baselines. We conclude that by introducing a novel linear dynamical prior, KoVAE improves generative results.

Table 4: Discriminative ablation results with regular and irregular 30% and 50% data on our method (KoVAE), without the linear prior ($\alpha = 0$), and also without the RNN ($\alpha = 0$, no GRU).

	regular				30%				50%			
	Sines	Stocks	Energy	MuJoCo	Sines	Stocks	Energy	MuJoCo	Sines	Stocks	Energy	MuJoCo
KoVAE	**0.005**	**0.009**	**0.143**	**0.076**	**0.035**	**0.162**	**0.280**	**0.123**	**0.030**	**0.092**	**0.298**	0.117
$\alpha = 0$	0.006	0.023	0.155	0.087	0.038	0.172	0.295	0.131	0.040	0.181	0.306	**0.108**
$\alpha = 0$, no GRU	-	-	-	-	0.268	0.272	0.436	0.267	0.275	0.225	0.444	0.305

6 CONCLUSION

Generative modeling of time series data is often modeled with GANs which are unstable to train and exhibit mode collapse. In contrast, VAEs are more robust to such issues, however, current generative time series approaches employ non-sequential prior models. Further, introducing constraints that impose domain knowledge is challenging in these frameworks. We propose Koopman VAE (KoVAE), a new variational autoencoder that is based on a novel dynamical linear prior. Our method enjoys the benefits of VAEs, it supports regular and irregular time series data, and it facilitates the incorporation of physics-constraints, and analysis through the lens of linear dynamical systems theory. We extensively evaluate our approach on generative benchmarks in comparison to strong baselines, and we show that KoVAE significantly outperforms existing work on several quantitative and qualitative metrics. We also demonstrate on a real-world challenging climate dataset that KoVAE approximates well the associated density distribution and it generates accurate temperature long-term signals. Future work will explore the utility of KoVAE for scientific and engineering problems in more depth.

REFERENCES

Ahmed Alaa, Alex James Chan, and Mihaela van der Schaar. Generative time-series modeling with Fourier flows. In *International Conference on Learning Representations*, 2020.

Yihao Ang, Qiang Huang, Yifan Bao, Anthony KH Tung, and Zhiyong Huang. TSGBench: time series generation benchmark. *arXiv preprint arXiv:2309.03755*, 2023.

Hassan Arbabi and Igor Mezic. Ergodic theory, dynamic mode decomposition, and computation of spectral properties of the Koopman operator. *SIAM Journal on Applied Dynamical Systems*, 16 (4):2096–2126, 2017.

Omri Azencot, Mirela Ben-Chen, Frédéric Chazal, and Maks Ovsjanikov. An operator approach to tangent vector field processing. In *Computer Graphics Forum*, volume 32, pp. 73–82. Wiley Online Library, 2013.

Omri Azencot, Steffen Weißmann, Maks Ovsjanikov, Max Wardetzky, and Mirela Ben-Chen. Functional fluids on surfaces. In *Computer Graphics Forum*, volume 33, pp. 237–246. Wiley Online Library, 2014.

Omri Azencot, Wotao Yin, and Andrea Bertozzi. Consistent dynamic mode decomposition. *SIAM Journal on Applied Dynamical Systems*, 18(3):1565–1585, 2019.

Omri Azencot, N Benjamin Erichson, Vanessa Lin, and Michael Mahoney. Forecasting sequential data using consistent Koopman autoencoders. In *International Conference on Machine Learning*, pp. 475–485. PMLR, 2020.

Nimrod Berman, Ilan Naiman, and Omri Azencot. Multifactor sequential disentanglement via structured Koopman autoencoders. In *The Eleventh International Conference on Learning Representations, ICLR*, 2023.

Tom Brown, Benjamin Mann, Nick Ryder, Melanie Subbiah, Jared D Kaplan, Prafulla Dhariwal, Arvind Neelakantan, Pranav Shyam, Girish Sastry, Amanda Askell, et al. Language models are few-shot learners. *Advances in neural information processing systems*, 33:1877–1901, 2020.

Steven L Brunton, Marko Budišić, Eurika Kaiser, and J Nathan Kutz. Modern Koopman theory for dynamical systems. *SIAM Rev.*, 2021.

Marko Budišić, Ryan Mohr, and Igor Mezić. Applied koopmanism. *Chaos: An Interdisciplinary Journal of Nonlinear Science*, 22(4), 2012.

Luis Candanedo. Appliances energy prediction. UCI Machine Learning Repository, 2017.

Zhengping Che, Sanjay Purushotham, Kyunghyun Cho, David Sontag, and Yan Liu. Recurrent neural networks for multivariate time series with missing values. *Scientific reports*, 8(1):6085, 2018.

Ricky TQ Chen, Yulia Rubanova, Jesse Bettencourt, and David K Duvenaud. Neural ordinary differential equations. *Advances in neural information processing systems*, 31, 2018.

Kyunghyun Cho, Bart van Merrienboer, Çaglar Gülçehre, Dzmitry Bahdanau, Fethi Bougares, Holger Schwenk, and Yoshua Bengio. Learning phrase representations using RNN encoder-decoder for statistical machine translation. In *Proceedings of the 2014 Conference on Empirical Methods in Natural Language Processing, EMNLP*, pp. 1724–1734. ACL, 2014.

Junyoung Chung, Kyle Kastner, Laurent Dinh, Kratarth Goel, Aaron C Courville, and Yoshua Bengio. A recurrent latent variable model for sequential data. *Advances in neural information processing systems*, 28, 2015.

Andrea Coletta, Sriram Gopalakrishan, Daniel Borrajo, and Svitlana Vyetrenko. On the constrained time-series generation problem. *arXiv preprint arXiv:2307.01717*, 2023.

Suddhasattwa Das and Dimitrios Giannakis. Delay-coordinate maps and the spectra of Koopman operators. *Journal of Statistical Physics*, 175(6):1107–1145, 2019.

Abhyuday Desai, Cynthia Freeman, Zuhui Wang, and Ian Beaver. TimeVAE: a variational auto-encoder for multivariate time series generation. *arXiv preprint arXiv:2111.08095*, 2021.

Carl Doersch. Tutorial on variational autoencoders. *arXiv preprint arXiv:1606.05908*, 2016.

Akshunna S Dogra and William Redman. Optimizing neural networks via Koopman operator theory. *Advances in Neural Information Processing Systems*, 33:2087–2097, 2020.

Chris Donahue, Julian McAuley, and Miller Puckette. Adversarial audio synthesis. In *International Conference on Learning Representations*, 2019.

Tanja Eisner, Bálint Farkas, Markus Haase, and Rainer Nagel. *Operator theoretic aspects of ergodic theory*, volume 272. Springer, 2015.

N Benjamin Erichson, Michael Muehlebach, and Michael W Mahoney. Physics-informed autoencoders for Lyapunov-stable fluid flow prediction. *arXiv preprint arXiv:1905.10866*, 2019.

Cristóbal Esteban, Stephanie L Hyland, and Gunnar Rätsch. Real-valued (medical) time series generation with recurrent conditional GANs. *arXiv preprint arXiv:1706.02633*, 2017.

Laurent Girin, Simon Leglaive, Xiaoyu Bie, Julien Diard, Thomas Hueber, and Xavier Alameda-Pineda. Dynamical variational autoencoders: A comprehensive review. *Found. Trends Mach. Learn.*, 15(1-2):1–175, 2021.

Ian Goodfellow. Nips 2016 tutorial: Generative adversarial networks. *arXiv preprint arXiv:1701.00160*, 2016.

Ian Goodfellow, Jean Pouget-Abadie, Mehdi Mirza, Bing Xu, David Warde-Farley, Sherjil Ozair, Aaron Courville, and Yoshua Bengio. Generative adversarial networks. *Advances in neural information processing systems*, 27, 2014.

Ian Goodfellow, Yoshua Bengio, and Aaron Courville. *Deep learning*. MIT press, 2016.

Anirudh Goyal, Alex Lamb, Ying Zhang, Saizheng Zhang, Aaron C. Courville, and Yoshua Bengio. Professor forcing: a new algorithm for training recurrent networks. In *Advances in Neural Information Processing Systems 29*, pp. 4601–4609, 2016.

Alex Graves. Generating sequences with recurrent neural networks. *arXiv preprint arXiv:1308.0850*, 2013.

Minghao Han, Jacob Euler-Rolle, and Robert K. Katzschmann. DeSKO: stability-assured robust control with a deep stochastic Koopman operator. In *The Tenth International Conference on Learning Representations, ICLR*, 2022.

Hans Hersbach, Bill Bell, Paul Berrisford, Shoji Hirahara, András Horányi, Joaquín Muñoz-Sabater, Julien Nicolas, Carole Peubey, Raluca Radu, Dinand Schepers, et al. The ERA5 global reanalysis. *Quarterly Journal of the Royal Meteorological Society*, 146(730):1999–2049, 2020.

Irina Higgins, Loic Matthey, Arka Pal, Christopher Burgess, Xavier Glorot, Matthew Botvinick, Shakir Mohamed, and Alexander Lerchner. beta-VAE: learning basic visual concepts with a constrained variational framework. In *International conference on learning representations*, 2016.

Ferenc Huszár. Variational inference using implicit distributions. *arXiv preprint arXiv:1702.08235*, 2017.

Daniel Jarrett, Ioana Bica, and Mihaela van der Schaar. Time-series generation by contrastive imitation. *Advances in Neural Information Processing Systems*, 34:28968–28982, 2021.

Jinsung Jeon, Jeonghak Kim, Haryong Song, Seunghyeon Cho, and Noseong Park. GT-GAN: general purpose time series synthesis with generative adversarial networks. *Advances in Neural Information Processing Systems*, 35:36999–37010, 2022.

Patrick Kidger, James Morrill, James Foster, and Terry Lyons. Neural controlled differential equations for irregular time series. *Advances in Neural Information Processing Systems*, 33:6696–6707, 2020.

Diederik P. Kingma and Max Welling. Auto-encoding variational bayes. In *2nd International Conference on Learning Representations, ICLR*, 2014.

Bernard O Koopman. Hamiltonian systems and transformation in Hilbert space. *Proceedings of the National Academy of Sciences*, 17(5):315–318, 1931.

Hongming Li, Shujian Yu, and José C. Príncipe. Causal recurrent variational autoencoder for medical time series generation. In *Thirty-Seventh AAAI Conference on Artificial Intelligence, AAAI*, pp. 8562–8570, 2023.

Xuechen Li, Ting-Kam Leonard Wong, Ricky TQ Chen, and David Duvenaud. Scalable gradients for stochastic differential equations. In *International Conference on Artificial Intelligence and Statistics*, pp. 3870–3882. PMLR, 2020.

Mario Lucic, Karol Kurach, Marcin Michalski, Sylvain Gelly, and Olivier Bousquet. Are GANs created equal? a large-scale study. *Advances in neural information processing systems*, 31, 2018.

Bethany Lusch, J Nathan Kutz, and Steven L Brunton. Deep learning for universal linear embeddings of nonlinear dynamics. *Nature communications*, 9(1):4950, 2018.

Alexandre Mauroy and Igor Mezić. A spectral operator-theoretic framework for global stability. In *52nd IEEE Conference on Decision and Control*, pp. 5234–5239. IEEE, 2013.

Alexandre Mauroy and Igor Mezić. Global stability analysis using the eigenfunctions of the Koopman operator. *IEEE Transactions on Automatic Control*, 61(11):3356–3369, 2016.

Igor Mezić. Analysis of fluid flows via spectral properties of the Koopman operator. *Annual Review of Fluid Mechanics*, 45:357–378, 2013.

Igor Mezic. Koopman operator spectrum and data analysis. *arXiv preprint arXiv:1702.07597*, 2017.

Olof Mogren. C-RNN-GAN: continuous recurrent neural networks with adversarial training. *arXiv preprint arXiv:1611.09904*, 2016.

Jeremy Morton, Freddie D. Witherden, and Mykel J. Kochenderfer. Deep variational Koopman models: inferring Koopman observations for uncertainty-aware dynamics modeling and control. In *Proceedings of the Twenty-Eighth International Joint Conference on Artificial Intelligence, IJCAI*, pp. 3173–3179, 2019.

Ilan Naiman and Omri Azencot. An operator theoretic approach for analyzing sequence neural networks. In *Proceedings of the AAAI conference on artificial intelligence*, volume 37, pp. 9268–9276, 2023.

Antonio Orvieto, Samuel L. Smith, Albert Gu, Anushan Fernando, Çaglar Gülçehre, Razvan Pascanu, and Soham De. Resurrecting recurrent neural networks for long sequences. In *International Conference on Machine Learning, ICML*, volume 202, pp. 26670–26698, 2023.

Shaowu Pan and Karthik Duraisamy. Physics-informed probabilistic learning of linear embeddings of nonlinear dynamics with guaranteed stability. *SIAM Journal on Applied Dynamical Systems*, 19(1):480–509, 2020.

Aditya Ramesh, Prafulla Dhariwal, Alex Nichol, Casey Chu, and Mark Chen. Hierarchical text-conditional image generation with clip latents. *arXiv preprint arXiv:2204.06125*, 1(2):3, 2022.

William T Redman, Maria Fonoberova, Ryan Mohr, Ioannis G Kevrekidis, and Igor Mezić. An operator theoretic view on pruning deep neural networks. In *The Tenth International Conference on Learning Representations, ICLR*, 2022.

Robin Rombach, Andreas Blattmann, Dominik Lorenz, Patrick Esser, and Björn Ommer. High-resolution image synthesis with latent diffusion models. In *Proceedings of the IEEE/CVF conference on computer vision and pattern recognition*, pp. 10684–10695, 2022.

Clarence W Rowley, Igor Mezić, Shervin Bagheri, Philipp Schlatter, and Dan S Henningson. Spectral analysis of nonlinear flows. *Journal of fluid mechanics*, 641:115–127, 2009.

Yulia Rubanova, Ricky TQ Chen, and David K Duvenaud. Latent ordinary differential equations for irregularly-sampled time series. *Advances in neural information processing systems*, 32, 2019.

Divya Saxena and Jiannong Cao. Generative adversarial networks (GANs) challenges, solutions, and future directions. *ACM Computing Surveys (CSUR)*, 54(3):1–42, 2021.

Peter J Schmid. Dynamic mode decomposition of numerical and experimental data. *Journal of fluid mechanics*, 656:5–28, 2010.

Jascha Sohl-Dickstein, Eric Weiss, Niru Maheswaranathan, and Surya Ganguli. Deep unsupervised learning using nonequilibrium thermodynamics. In *International conference on machine learning*, pp. 2256–2265. PMLR, 2015.

Anand Srinivasan and Naoya Takeishi. An MCMC method for uncertainty set generation via operator-theoretic metrics. In *59th IEEE Conference on Decision and Control, CDC*, pp. 2714–2719, 2020.

Steven H Strogatz. *Nonlinear dynamics and chaos with student solutions manual: With applications to physics, biology, chemistry, and engineering*. CRC press, 2018.

Naoya Takeishi, Yoshinobu Kawahara, and Takehisa Yairi. Learning Koopman invariant subspaces for dynamic mode decomposition. *Advances in neural information processing systems*, 30, 2017.

Kshitij Tayal, Arvind Renganathan, Rahul Ghosh, Xiaowei Jia, and Vipin Kumar. Koopman invertible autoencoder: Leveraging forward and backward dynamics for temporal modeling. *arXiv preprint arXiv:2309.10291*, 2023.

Emanuel Todorov, Tom Erez, and Yuval Tassa. MuJoCo: a physics engine for model-based control. In *2012 IEEE/RSJ International Conference on Intelligent Robots and Systems*, pp. 5026–5033. IEEE, 2012. doi: 10.1109/IROS.2012.6386109.

Aäron van den Oord, Sander Dieleman, Heiga Zen, Karen Simonyan, Oriol Vinyals, Alex Graves, Nal Kalchbrenner, Andrew W. Senior, and Koray Kavukcuoglu. WaveNet: a generative model for raw audio. In *The 9th ISCA Speech Synthesis Workshop*, pp. 125, 2016.

Laurens Van der Maaten and Geoffrey Hinton. Visualizing data using t-sne. *Journal of machine learning research*, 9(11), 2008.

Rui Wang, Yihe Dong, Sercan Ö. Arik, and Rose Yu. Koopman neural forecaster for time series with temporal distribution shifts. In *The Eleventh International Conference on Learning Representations, ICLR*, 2023.

Tianlin Xu, Li Kevin Wenliang, Michael Munn, and Beatrice Acciaio. COT-GAN: generating sequential data via causal optimal transport. *Advances in neural information processing systems*, 33:8798–8809, 2020.

Jinsung Yoon, Daniel Jarrett, and Mihaela Van der Schaar. Time-series generative adversarial networks. *Advances in neural information processing systems*, 32, 2019.

Ailing Zeng, Muxi Chen, Lei Zhang, and Qiang Xu. Are transformers effective for time series forecasting? In *Proceedings of the AAAI conference on artificial intelligence*, pp. 11121–11128, 2023.

Linqi Zhou, Michael Poli, Winnie Xu, Stefano Massaroli, and Stefano Ermon. Deep latent state space models for time-series generation. In *International Conference on Machine Learning*, pp. 42625–42643. PMLR, 2023.

Harrison Zhu, Carles Balsells-Rodas, and Yingzhen Li. Markovian Gaussian process variational autoencoders. In *International Conference on Machine Learning*, pp. 42938–42961. PMLR, 2023.

A   STATIC VARIATIONAL AUTOENCODERS.

We recall a few governing equations from (Kingma & Welling, 2014; Doersch, 2016). In generative modeling, we want to compute the probability density function (PDF) $P(x)$ using a *maximum likelihood* framework. The density $P(x)$ reads

$$P(x) = \int p(x|z;\theta)p(z)\,\mathrm{d}\,z\,, \tag{12}$$

where z is a latent representation associated with x. The model $p(x|z;\theta)$ ideally approaches x for some z. In variational inference, we typically have that $p(x|z;\theta) = \mathcal{N}(x|f(z;\theta),\sigma^2 I)$, i.e., a Gaussian distribution where the mean is generated with a neural network f. However, two issues arise with the above PDF: 1) how to define z; and 2) how to integrate over z.

VAEs provide a solution for both issues. The first issue is resolved by assuming that z is drawn from a predefined distribution, e.g., $\mathcal{N}(0,I)$. The second issue can be potentially solved by approximating Eq. 12 with a sum, i.e., $P(x) \approx \frac{1}{n}\sum_i p(x|z_i)$. A challenge, however, is that n needs to be huge in high-dimensions. Instead, we observe that for most z, the term $p(x|z)$ will be nearly zero, and thus we can focus on sampling z that are likely to produce x. Consequently, we need an approximate posterior $q(z|x)$ which allows to compute $\mathbb{E}_{z\sim q}p(x|z)$, where z is obtained using the re-parametrization trick.

To guide training so that the prior and approximate posterior match, we employ the Kullback–Liebler Divergence $\mathrm{KL}[\cdot \,\|\, \cdot]$ between $q(z)$ and $p(z|x)$. The model is trained using the evidence lower bound (ELBO) loss $\mathbb{E}_{z\sim q}[\log p(x|z)] - \mathrm{KL}[q(z|x)\,\|\,p(z)]$, which is one of the core equations of VAE. Notice that the objective takes the form of reconstruction and regularization penalties, respectively.

B   NEURAL CONTROLLED DIFFERENTIAL EQUATIONS

Irregularly sampled TS information $x_{t_1:t_N}$ for, e.g., $t_j \in [1,\ldots,T]$ cannot be modeled directly with discrete-time architectures such as recurrent neural networks (RNN). Therefore, the continuous analog of RNN is considered for $x_{t_1:t_N}$ based on neural controlled differential equations (NCDE) (Kidger et al., 2020) that are given by

$$h(t_{i+1}) = h(t_i) + \int_{t_i}^{t_{i+1}} f(h(t)\,;\,\theta_f)\,\mathrm{d}\,X(t)\,, \tag{13}$$

where $h(t_i)$ is the hidden code associated with x_{t_i}, $X(t)$ is a continuous-time trajectory generated from $x_{t_1:t_N}$ via an interpolation method with $X(t_i) := x_{t_i}$, and f is a neural network parametrized by θ_f whose role is to learn the latent infinitesimal factor.

C   LOSS FUNCTION EVALUATION

Our model is trained using the objective function $\mathcal{L}$, defined in Eq. 8, and repeated below,

$$\mathcal{L} = \mathbb{E}_{z_{1:T}\sim q}[\log p(x_{t_1:t_N}|z_{1:T})] + \alpha\mathcal{L}_{\mathrm{pred}}(z_{1:T},\bar{z}_{1:T}) - \beta\mathrm{KL}[q(z_{1:T}|x_{t_1:t_N})\,\|\,p(z_{1:T})]\,,$$

where the first addend is the reconstruction term, the second addend is the predictive loss term, and the last addend is the KL regularization term. To evaluate $\mathcal{L}$ in practice, we make a few standard assumptions, followed by straightforward computations. First, we assume that $p(x_{1:T}|z_{1:T})$ follows a Gaussian distribution whose mean is the output of the model and its variance is some constant. Namely, $p(x_{1:T}|z_{1:T}) = \mathcal{N}\big(x_{1:T}\,;\,\tilde{x}_{1:T}(z_{1:T},\theta),\sigma^2\big)$, where $\tilde{x}_{1:T}(z_{1:T})$ denotes the output of the decoder whose learnable parameters are given by θ. This is a common probabilistic assumption (Goodfellow et al., 2016), under which the term $\mathbb{E}_{z_{1:T}\sim q}[\log p(x_{1:T}|z_{1:T})]$ becomes a simple mean squared error (MSE) between $x_{1:T}$ and $\tilde{x}_{1:T}$. Second, a similar reasoning is applied to $\mathcal{L}_{\mathrm{pred}}$, yielding an MSE evaluation between $z_{1:T}$ and $\bar{z}_{1:T}$. Finally, the regularization term involves the distribution $p(z_{1:T}) := \delta(z_{1:T} - A\bar{z}_{1:T})p(\bar{z}_{1:T})$, where $\delta(\cdot)$ is the Dirac delta distribution. However, the KL divergence is always evaluated in our framework on batches $z_{1:T}$ computed from $\bar{z}_{1:T}$. Therefore, we approximate $\delta(z_{1:T} - A\bar{z}_{1:T})$ by 1, leading to $p(z_{1:T}) \approx p(\bar{z}_{1:T})$. Then, we can compute the KL term using a closed-form formulation given the mean and variance of two distributions.

D   VARIATIONAL PENALIZED EVIDENCE LOWER BOUND

In what follows, we present the derivation of the variational penalized evidence lower bound for our method. Our objective is to minimize $KL[q(z_{\leq T}|x_{\leq T})||p(z_{\leq T}|x_{\leq T})]$ under the Koopman constraint $\mathcal{L}_{\text{pred}}(z_{\leq T}, \bar{z}_{\leq T}) = \mathbb{E}_{\bar{z}_{\leq T} \sim p}[\log p(z_{\leq T}|\bar{z}_{\leq T})]$.

$$KL[q(z_{\leq T}|x_{\leq T})||p(z_{\leq T}|x_{\leq T})] + \mathbb{E}_{\bar{z}_{\leq T} \sim p}[\log p(z_{\leq T}|\bar{z}_{\leq T})]$$

$$= \int q(z_{\leq T}|x_{\leq T}) \log \frac{q(z_{\leq T}|x_{\leq T})}{p(z_{\leq T}|x_{\leq T})} dz_{\leq T} + \mathbb{E}_{\bar{z}_{\leq T} \sim p}[\log p(z_{\leq T}|\bar{z}_{\leq T})]$$

$$= \int q(z_{\leq T}|x_{\leq T}) \log \frac{q(z_{\leq T}|x_{\leq T})p(x_{\leq T})}{p(z_{\leq T}, x_{\leq T})} dz_{\leq T} + \mathbb{E}_{\bar{z}_{\leq T} \sim p}[\log p(z_{\leq T}|\bar{z}_{\leq T})]$$

$$= \int q(z_{\leq T}|x_{\leq T})[\log p(x_{\leq T}) + \log \frac{q(z_{\leq T}|x_{\leq T})}{p(z_{\leq T}, x_{\leq T})}] dz_{\leq T} + \mathbb{E}_{\bar{z}_{\leq T} \sim p}[\log p(z_{\leq T}|\bar{z}_{\leq T})]$$

$$= \log p(x_{\leq T}) + \int q(z_{\leq T}|x_{\leq T}) \log \frac{q(z_{\leq T}|x_{\leq T})}{p(z_{\leq T}, x_{\leq T})} dz_{\leq T} + \mathbb{E}_{\bar{z}_{\leq T} \sim p}[\log p(z_{\leq T}|\bar{z}_{\leq T})]$$

$$= \log p(x_{\leq T}) + \int q(z_{\leq T}|x_{\leq T}) \log \frac{q(z_{\leq T}|x_{\leq T})}{p(z_{\leq T})p(x_{\leq T}|z_{\leq T})} dz_{\leq T} + \mathbb{E}_{\bar{z}_{\leq T} \sim p}[\log p(z_{\leq T}|\bar{z}_{\leq T})]$$

$$= \log p(x_{\leq T}) + \int q(z_{\leq T}|x_{\leq T})[\log \frac{q(z_{\leq T}|x_{\leq T})}{p(z_{\leq T})} - \log p(x_{\leq T}|z_{\leq T})] dz_{\leq T} + \mathbb{E}_{\bar{z}_{\leq T} \sim p}[\log p(z_{\leq T}|\bar{z}_{\leq T})]$$

$$= \log p(x_{\leq T}) + \mathbb{E}_{z_{\leq T} \sim q(z_{\leq T}|x_{\leq T})}[\log \frac{q(z_{\leq T}|x_{\leq T})}{p(z_{\leq T})} - \log p(x_{\leq T}|z_{\leq T})] + \mathbb{E}_{\bar{z}_{\leq T} \sim p}[\log p(z_{\leq T}|\bar{z}_{\leq T})]$$

$$= \log p(x_{\leq T}) + KL[q(z_{\leq T}|x_{\leq T})||p(z_{\leq T})] - \mathbb{E}_{z_{\leq T} \sim q(z_{\leq T}|x_{\leq T})}[\log p(x_{\leq T}|z_{\leq T})] + \mathbb{E}_{\bar{z}_{\leq T} \sim p}[\log p(z_{\leq T}|\bar{z}_{\leq T})]$$

Thus we have the following:

$$KL[q(z_{\leq T}|x_{\leq T})||p(z_{\leq T}|x_{\leq T})] + \mathbb{E}_{\bar{z}_{\leq T} \sim p}[\log p(z_{\leq T}|\bar{z}_{\leq T})] =$$
$$\log p(x_{\leq T}) + KL[q(z_{\leq T}|x_{\leq T})||p(z_{\leq T})] - \mathbb{E}_{z_{\leq T} \sim q(z_{\leq T}|x_{\leq T})}[\log p(x_{\leq T}|z_{\leq T})] + \mathbb{E}_{\bar{z}_{\leq T} \sim p}[\log p(z_{\leq T}|\bar{z}_{\leq T})]$$

Now, rearranging the equation, we yield:

$$\log p(x_{\leq T}) - KL[q(z_{\leq T}|x_{\leq T})||p(z_{\leq T}|x_{\leq T})] + \mathbb{E}_{\bar{z}_{\leq T} \sim p}[\log p(z_{\leq T}|\bar{z}_{\leq T})] =$$
$$- \mathbb{E}_{z_{\leq T} \sim q(z_{\leq T}|x_{\leq T})}[\log p(x_{\leq T}|z_{\leq T})] + KL[q(z_{\leq T}|x_{\leq T})||p(z_{\leq T})] + \mathbb{E}_{\bar{z}_{\leq T} \sim p}[\log p(z_{\leq T}|\bar{z}_{\leq T})]$$

Thus finally:

$$\log p(x_{\leq T}) + \mathbb{E}_{\bar{z}_{\leq T} \sim p}[\log p(z_{\leq T}|\bar{z}_{\leq T})] \leq \tag{14}$$
$$- \mathbb{E}_{z_{\leq T} \sim q(z_{\leq T}|x_{\leq T})}[\log p(x_{\leq T}|z_{\leq T})] + KL[q(z_{\leq T}|x_{\leq T})||p(z_{\leq T})] + \mathbb{E}_{\bar{z}_{\leq T} \sim p}[\log p(z_{\leq T}|\bar{z}_{\leq T})]$$

E   DATASETS AND BASELINE METHODS

We consider four synthetic and real-world datasets with different characteristic properties and statistical features, following challenging benchmarks on generative time series (Yoon et al., 2019; Jeon et al., 2022). **Sines**, is a multivariate simulated data, where each sample $x_t^i(j) := \sin(2\pi\eta t + \theta)$, with $\eta \sim \mathcal{U}[0,1]$, $\theta \sim \mathcal{U}[-\pi, \pi]$, and channel $j \in \{1, ..., 5\}$ for every i in the dataset. This dataset is characterized by its continuity and periodic properties. **Stocks**, consists of the daily historical Google stocks data from 2004 to 2019 and has six channels including high, low, opening, closing, and adjusted closing prices and the volume. In contrast to Sines, Stocks is assumed to include random walk patterns and it is generally aperiodic. **Energy**, is a multivariate UCI appliance energy prediction dataset (Candanedo, 2017), with 28 channels, correlated features, and it is characterized by noisy periodicity and continuous-valued measurements. Finally, **MuJoCo** (**Mu**lti-**Jo**int dynamics with **Co**ntact) (Todorov et al., 2012), is a general-purpose physics generator, which we use to simulate time series data with 14 channels.

We compare our method with several state-of-the-art (SOTA) generative time series models, such as TimeGAN (Yoon et al., 2019), RCGAN (Esteban et al., 2017), C-RNN-GAN (Mogren, 2016), WaveGAN (Donahue et al., 2019), WaveNet (van den Oord et al., 2016), T-Forcing (Graves, 2013), P-Forcing (Goyal et al., 2016), TimeVAE (Desai et al., 2021), CR-VAE (Li et al., 2023), and the recent irregular method GT-GAN (Jeon et al., 2022). All the methods, except for GT-GAN, are not designed to handle missing observations; thus, we follow GT-GAN and compare them with their re-designed versions. Specifically, extending regular approaches to support irregular TS requires the conversion of a dynamical module to its time-continuous version. For instance, we converted GRU layers to GRU-Δt and GRU-D to exploit the time difference between observations and to learn the exponential decay between samples, respectively. We denote the re-designed methods by adding Δt or D postfix to their name, such as TimeGAN-Δt and TimeGAN-D.

F   CONSTRAINED GENERATION AND ANALYSIS

In addition to the analysis of the constrained system in Eq. 10, we also compute the approximate Koopman operators for all the regular systems we consider in the main text. Specifically, we show in Fig. 5 four panels, corresponding to the spectral eigenvalue plots for Sines (left), Stocks (middle left), Energy (middle right), and MuJoCo (right). Green eigenvalues are within the unit circle, whereas red eigenvalues are located outside the unit circle. Noticeably, the learned dynamics for Sines, Stocks and MuJoCo are stable, i.e., their corresponding eigenvalues are within the unit circle, and thus, their training, inference and overall long-term behavior is expected to be numerically stable and not produce values that present large deviations. In contrast, the spectrum associated with the model learned for the Energy dataset reveals unstable dynamics where the largest $\lambda_i \gg 1$. We hypothesize that we can benefit from incorporating spectral constraints to regularize the dynamics and achieve stable dynamics. In the future, we will investigate whether spectral constraints can enhance the generation results and overall behavior of such models.
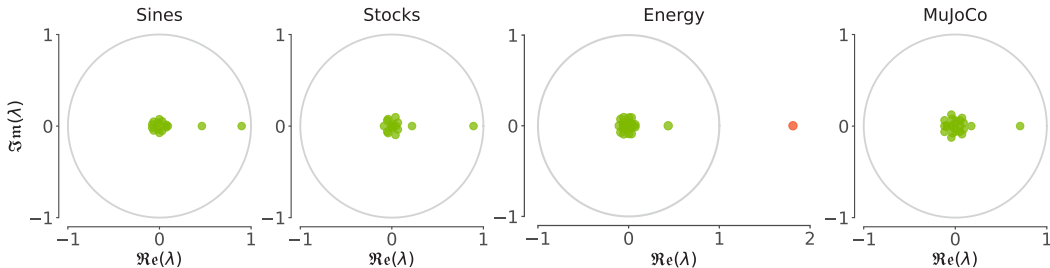

Figure 5: The spectral distribution of the approximate Koopman operator of the prior for each dataset in the regular setting.
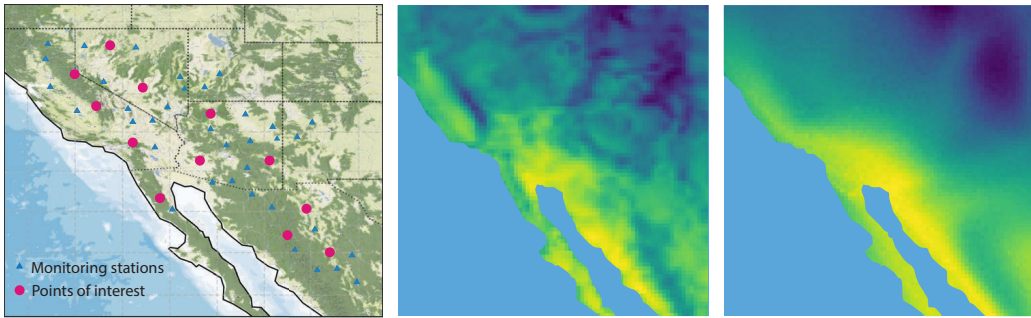
Figure 6: Comparison of the temporally-averaged temperature distribution of the generated signals and ground truth data in California region. left: California region map. middle: ground truth average. right: generated average.

G CONDITIONAL GENERATION FOR WEATHER DATA

Accurate weather data is essential for various applications, such as agriculture, water resource management, and disaster early warning. However, due to the limited availability of weather stations, scientists are faced with the challenge of the inherent sparsity of observational weather data, especially in specific geographical areas of interest. Generative models can produce synthetic weather data to supplement sparse or incomplete observational datasets. In this paper, we explore the potential of our KoVAE model for modeling temperature dynamics based on sparse measurement data. Our objective is to generate the temperature data at any location within a specific region of interest. Hence, the proposed KoVAE model here is conditioned on the geospatial coordinates of the specific region. By leveraging conditional generative models, we hope to provide valuable insights into weather dynamics in specific regions and enhance the decision-making processes that are reliant on accurate weather information. Our model is trained with geospatial coordinates as conditional variables. To support the conditional training and generation, we made two simple modifications: (i) we add a very simple MLP to support spatial embeddings s; and (ii) we augment the decoder and prior to support conditional generation: $p(x_{t_1:t_N}|z_{1:T}, s)$ and $p(x_{1:T}, z_{1:T}, s) = p(z_{1:T}|s)p(x_{1:T}|z_{1:T}, s)$.

We focus on two representative regions in the United States: California and Central America areas. California has diverse and non-stationary weather changes due to the complex interactions between seas, lands, and mountains. Central America areas present more stable and relatively easier temperature dynamics compared with the California region. Both of these regions include a grid of 80×80, which means we have 6400 time series samples in total. Moreover, the dataset in this task comprises temperature at 2-meter height above the surface from ERA5 reanalysis dataset (Hersbach et al., 2020). We select 4-month observation data within the specific area for training and evaluating our VAE model. It contains 120 time steps for each time series sample. We split the train and test sets with a ratio of 80% and 20%. The generated time series samples are shown in Fig. 9 and Fig. 10. We can see that our KoVAE model can accurately capture the underlying dynamics of temperature data in both California and Central America regions. Furthermore, Fig. 6 and Fig. 7 exhibit the comparisons of the temporally-averaged temperature distribution between the generations and ground truth in California and Central America regions. The left panels in these figures show the points of interest with respect to the given monitoring stations, which can be used to condition our model. The temperature distribution patterns of the generations align well with those of the ground truth in the entire domain. Similarly, we also observe that the generation and ground truth match well when comparing minimum and maximum values over time, as shown in Fig. 8. Nevertheless, the fine-scale spatial details are lacking in our generation due to the absence of spatial constraints. In the future, we will enhance our conditional KoVAE model by incorporating spatial continuity and prior knowledge for spatiotemporal generation.
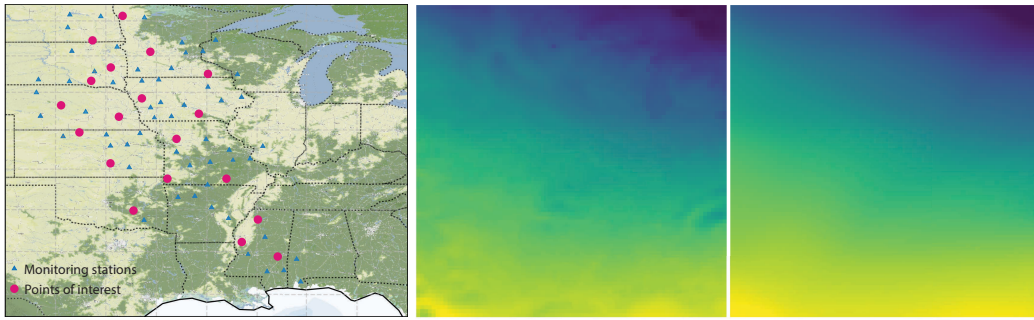
Figure 7: Comparison of the temporally-averaged temperature distribution between the generations and ground truth in Central America region. left: Central America region map. middle: ground truth average. right: generated average.

H ADDITIONAL GENERATION RESULTS

For brevity, in the main text, we provided tables without standard deviation (std). In this section, we provide extended tables that include the std for each metric. Tab. 6 and Tab. 7 present the results for the regular observed data of discriminative and predictive scores, respectively. In Tab. 8, Tab. 9, and Tab. 10 we show the results for the irregular sampled of 30%, 50%, and 70% missing observation, respectively. Each table includes both discriminative and predictive scores. Furthermore, we provide qualitative results to compare our model with GT-GAN, the second-best generation model for both regularly and irregularly sampled data. In Fig. 11 Fig. 12, Fig. 13, we visualize the t-SNE projection of both ground truth data and generated data (first row) and the PDF of ground truth data vs. generated data (second row). We perform the visualization for all regularly and irregularly sampled datasets.
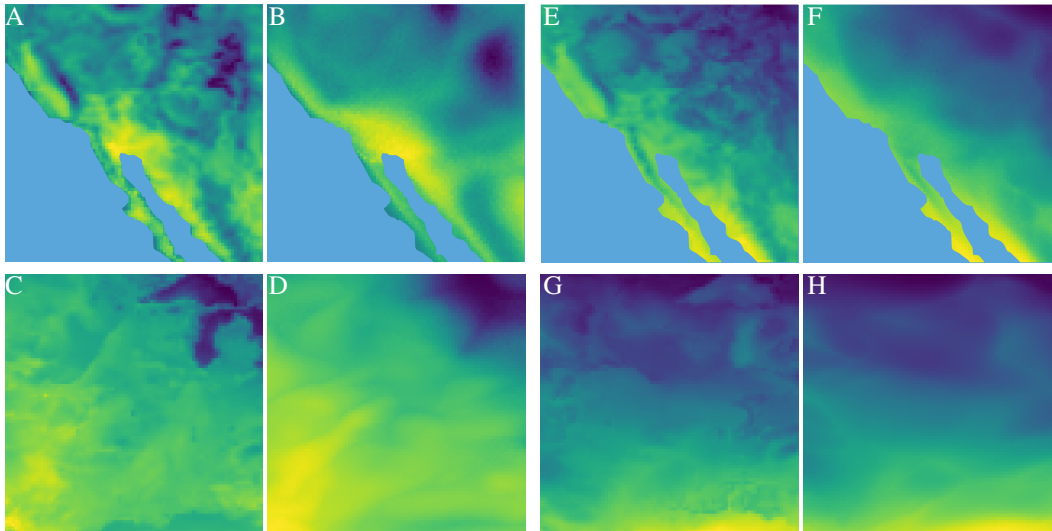

Figure 8: The maximum and minimum plots for both California and Central America regions. (A) The maximum value over time of the ground truth in the California region. (B) The maximum value over time of the generation in the California region. (C) The maximum value over time of the ground truth in the Central America region. (D) The maximum value over time of the generation in the Central America region. (E) The minimum value over time of the ground truth in the California region. (F) The minimum value over time of the generation in the California region. (G) The minimum value over time of the ground truth in the Central America region. (H) The minimum value over time of the generation in the Central America region.
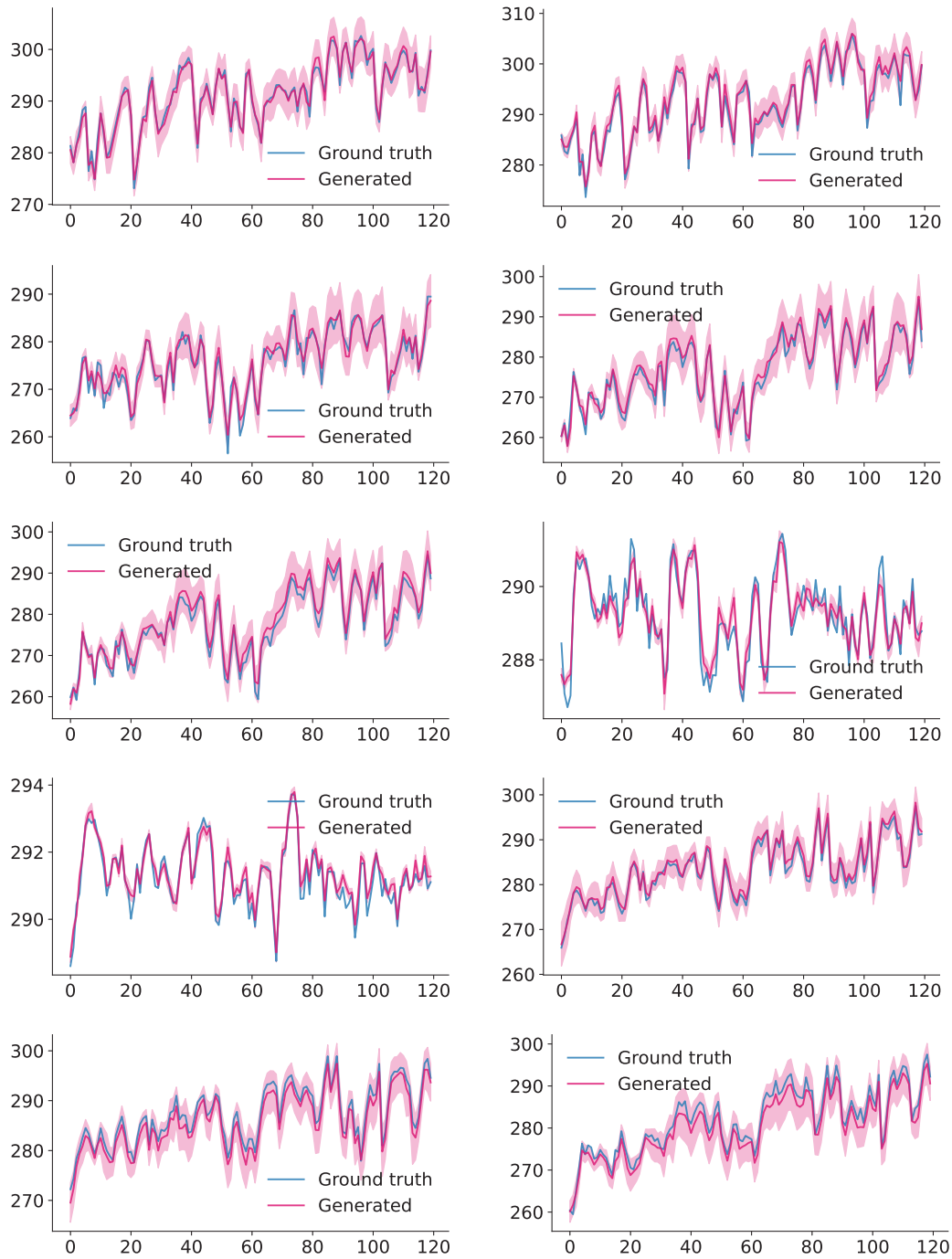
Figure 9: The representative generations in the California area.

I COMPUTATIONAL RESOURCES

Here we compare the model complexity (number of parameters), and the wall clock time measurement with GT-GAN. We present the details in Tab. 5. Both models were trained on the same software and hardware for fair comparison. The software environments we use are: CentOS Linux 7 (Core) and PYTHON 3.9.16, and the hardware is: NVIDIA RTX 3090. We observe that we use

20

Figure 10: The representative generations in the Central America area.

more parameters on the Energy and MuJoCo datasets, but the training time is significantly faster on the same software and hardware.

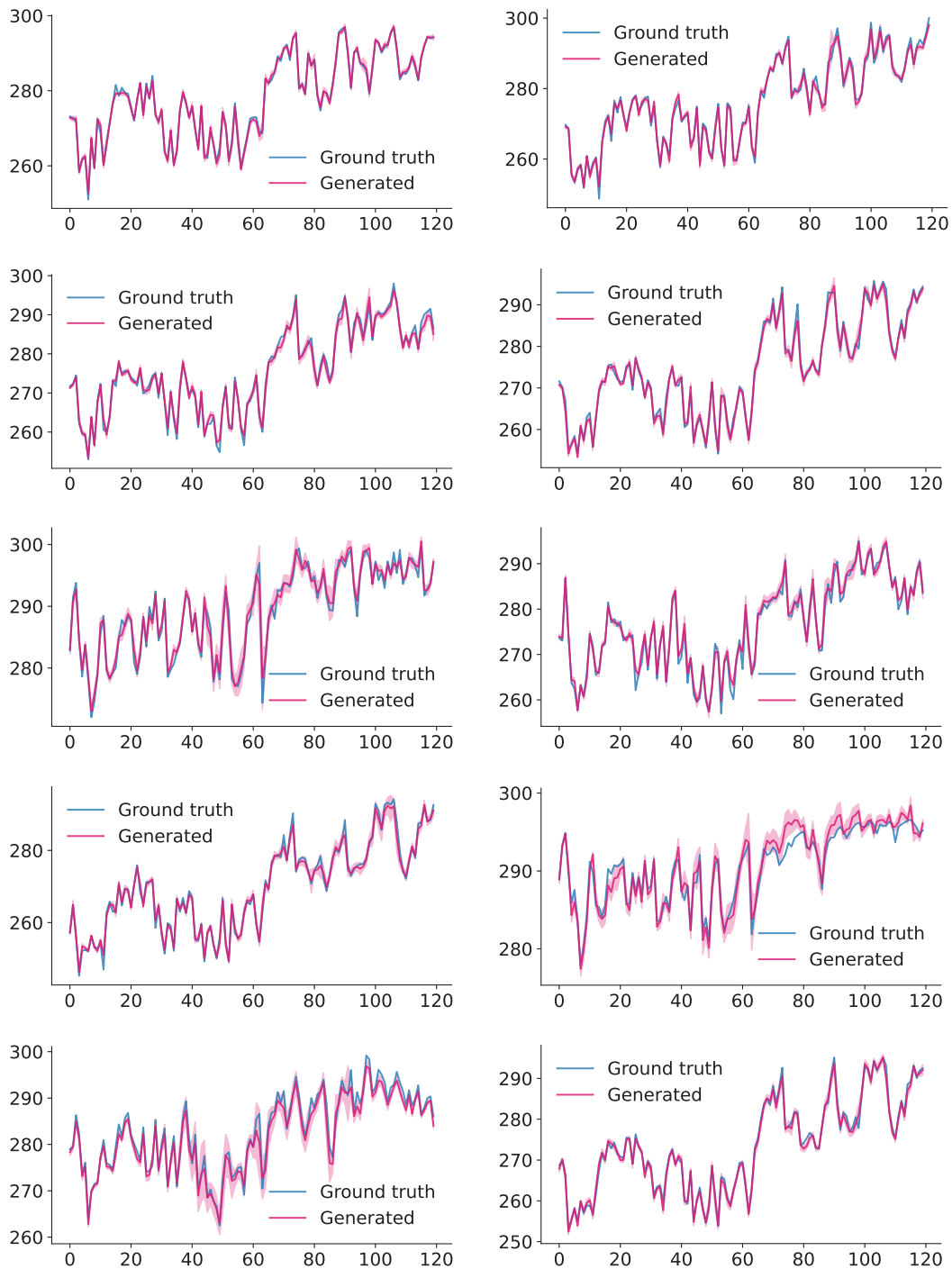| Method	Copm.	Sines	Stocks	Energy	MuJoCo
KoVAE (Ours)	# Parameters	**32,929**	**33,410**	230,860	195,902
	Wall Clock Time	**2h 49m**	**2h 49m**	**5h 16m**	**3h 46m**
GT-GAN	# Parameters	41,913	41,776	**57,104**	**47,346**
	Wall Clock Time	10h 12m	12h 20m	10h 39m	13h 12m

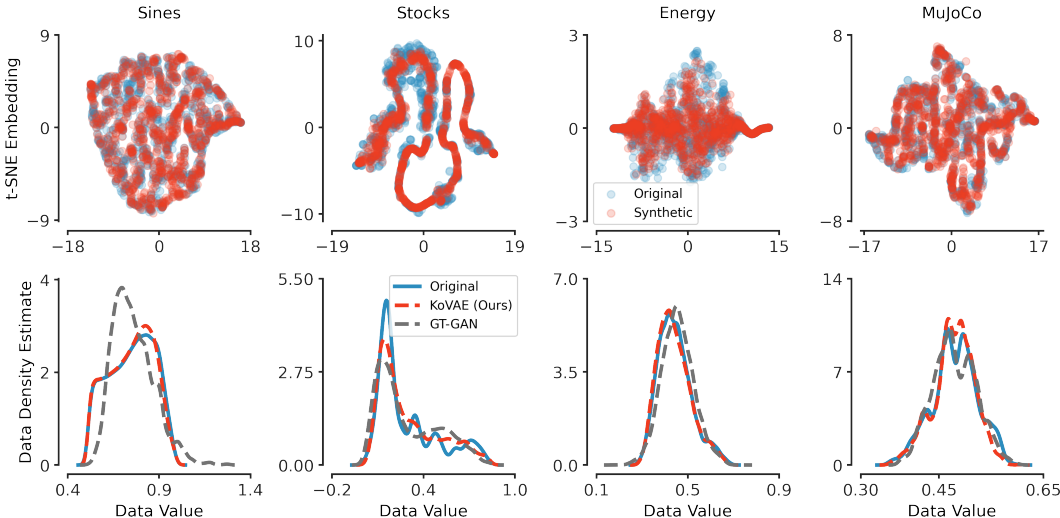Table 5: Comparison of number (#) of parameters and wall clock time.

Figure 11: We qualitatively evaluate our approach on regularly sampled data with two-dimensional t-SNE plots of the synthetic and real data (top row). In addition, we show the probability density functions of the real data, and for KoVAE and GT-GAN synthetic distributions (bottom row).

J HYPERPARAMETERS ROBUSTNESS

We also explore how stable our model is to hyperparameter choice. To this end, we perform an extensive grid search over the following space for:

$$\alpha, \beta \in \{1.0, 0.9, 0.7, 0.5, 0.3, 0.1, 0.09, 0.07, 0.05, 0.03, 0.01,$$

$$0.009, 0.007, 0.005, 0.003, 0.001, 0.0009, 0.0007, 0.0005\}^2$$

for the stocks dataset. Fig. 14 shows the discriminative score for each combination of α and β. Most of the values are lower than the second-best model for this task.

K RECONSTRUCTION RESULTS

In addition to studying the generative capabilities of KoVAE, we also investigate its reconstruction and inference features below. We show in Fig. 15 the reconstructed signals in the regular setting. Each subplot represent a separate feature, where for datasets with more than five channels, we plot the first five features. Solid lines represent ground-truth data, whereas dashed lines are the reconstructions our model outputs. For simplicity, we omitted axis labels. For all subplots, the x-axis represents time, and the y-axis is the feature values. Moreover, we also plot in Fig. 16 the inferred signals in the irregular 50% setting. In this case, half of the signal is removed during training, and thus, the reconstructions present the inference capabilities of our model. Our results indicate that KoVAE is able to successfully reconstruct and infer the data.

Figure 12: We qualitatively evaluate our approach on 30% irregularly sampled data with two-dimensional t-SNE plots of the synthetic and real data (top row). In addition, we show the probability density functions of the real data, and for KoVAE and GT-GAN synthetic distributions (bottom row).
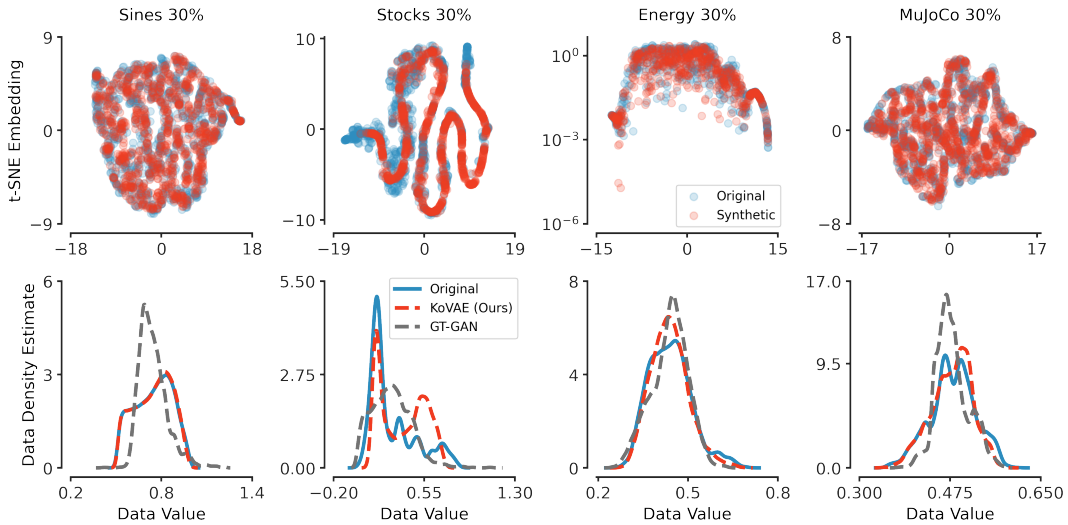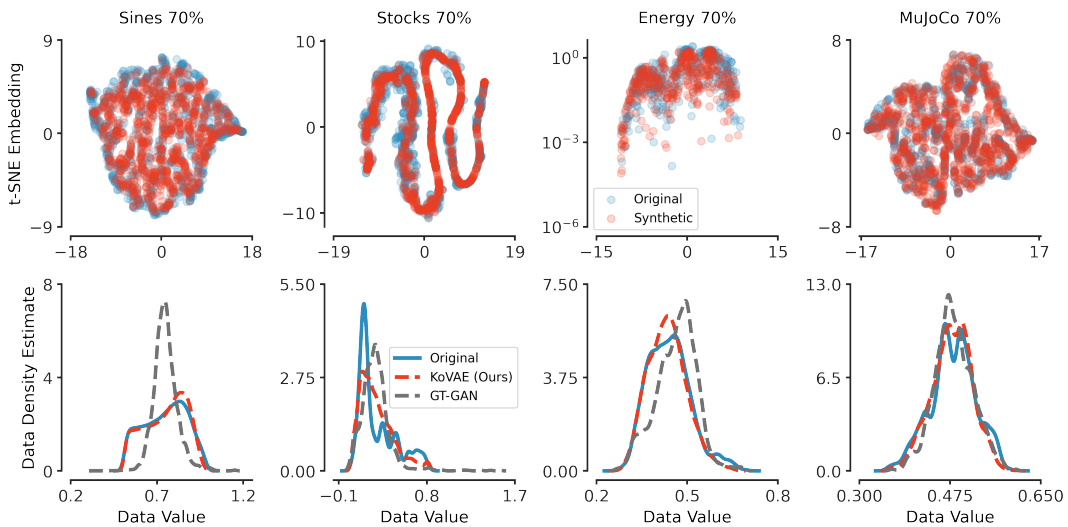

Figure 13: We qualitatively evaluate our approach on 70% irregularly sampled data with two-dimensional t-SNE plots of the synthetic and real data (top row). In addition, we show the probability density functions of the real data, and for KoVAE and GT-GAN synthetic distributions (bottom row).
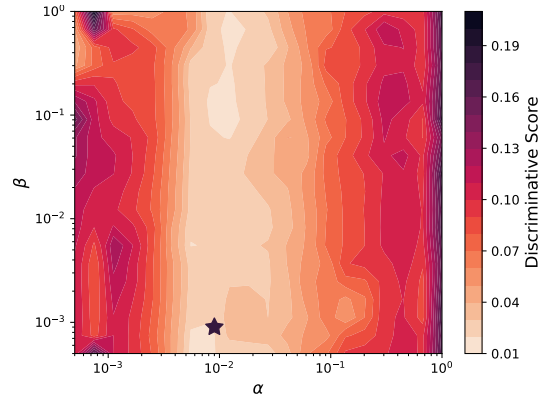
Figure 14: Each point in this plot represents the discriminative score for stocks regularly sampled data set when trained with specific α and β values. The star marker denotes the best discriminative score for some $\alpha = 9\mathrm{e}{-3}, \beta = 9\mathrm{e}{-4}$ values. In addition, most of the values in the figure present better performance than the second-best method.

Table 6: Regular TS, discriminative task

Method	Sines	Stocks	Energy	MuJoCo
KoVAE (Ours)	**.005±.003**	**.009±.006**	**.143±.011**	**.076±.017**
GT-GAN	.012±.014	.077±.031	.221±.068	.245±.029
TimeGAN	.011±.008	.102±.021	.236±.012	.409±.028
TimeVAE	.016±.010	.036±.033	.323±.029	.224±.026
CR-VAE	.342±.157	.320±.095	.475±.054	.464±.012
RCGAN	.022±.008	.196±.027	.336±.017	.436±.012
C-RNN-GAN	.229±.040	.399±.028	.499±.001	.412±.095
T-Forcing	.495±.001	.226±.035	.483±.004	.499±.000
P-Forcing	.430±.227	.257±.026	.412±.006	.500±.000
WaveNet	.158±.011	.232±.028	.397±.010	.385±.025
WaveGAN	.277±.013	.217±.022	.363±.012	.357±.017
RI	**54.54%**	**75.00%**	**35.29%**	**66.07%**

Table 7: Regular TS, predictive task

Method	Sines	Stocks	Energy	MuJoCo
KoVAE (Ours)	**.093±.000**	**.037±.000**	**.251±.000**	**.038±.002**
GT-GAN	.097±.000	.040±.000	.312±.002	.055±.000
TimeVAE	**.093±.000**	.037±.033	.254±.000	.039±.002
TimeGAN	.093±.019	.038±.001	.273±.004	.082±.006
CR-VAE	.143±.002	.076±.013	.277±.001	.050±.000
RCGAN	.097±.001	.040±.001	.292±.005	.081±.003
C-RNN-GAN	.127±.004	.038±.000	.483±.005	.055±.004
T-Forcing	.150±.022	.038±.001	.315±.005	.142±.014
P-Forcing	.116±.004	.043±.001	.303±.006	.102±.013
WaveNet	.117±.008	.042±.001	.311±.005	.333±.004
WaveGAN	.134±.013	.041±.001	.307±.007	.324±.006
Original	0.094	0.036	0.250	0.031

Table 8: Irregular time series (30% dropped)

	Method	Sines	Stocks	Energy	MuJoCo
Discriminative Score	VKAE (Ours)	**.035±.023**	**.162±.068**	**.280±.018**	**.123±.018**
	GT-GAN	.363±.063	.251±.097	.333±.063	.249±.035
	TimeGAN-$\triangle t$	.494±.012	.463±.020	.448±.027	.471±.016
	RCGAN-$\triangle t$	.499±.000	.436±.064	.500±.000	.500±.000
	C-RNN-GAN -$\triangle t$	.500±.000	.500±.001	.500±.000	.500±.000
	T-Forcing-$\triangle t$	.395±.063	.305±.002	.477±.011	.348±.041
	P-Forcing-$\triangle t$	.344±.127	.341±.035	.500±.000	.493±.010
	TimeGAN-D	.496±.008	.411±.040	.479±.010	.463±.025
	RCGAN-D	.500±.000	.500±.000	.500±.000	.500±.000
	C-RNN-GAN-D	.500±.000	.500±.000	.500±.000	.500±.000
	T-Forcing-D	.408±.087	.409±.051	.347±.046	.494±.004
	P-Forcing-D	.500±.000	.480±.060	.491±.020	.500±.000
Predictive Score	KoVAE (Ours)	**.074±.005**	**.019±.001**	**.049±.002**	**.043±.000**
	GT-GAN	.099±.004	.021±.003	.066±.001	.048±.001
	TimeGAN-$\triangle t$	.145±.025	.087±.001	.375±.011	.118±.032
	RCGAN-$\triangle t$	.144±.028	.181±.014	.351±.056	.433±.021
	C-RNN-GAN-$\triangle t$	.754±.000	.091±.007	.500±.000	.447±.000
	T-Forcing-$\triangle t$	.116±.002	.070±.013	.251±.000	.056±.001
	P-Forcing-$\triangle t$	.102±.002	.083±.018	.255±.001	.089±.011
	TimeGAN-D	.192±.082	.105±.053	.248±.024	.098±.006
	RCGAN-D	.388±.113	.523±.020	.409±.020	.361±.073
	C-RNN-GAN-D	.664±.001	.345±.002	.440±.000	.457±.001
	T-Forcing-D	.100±.002	.027±.002	.090±.001	.100±.001
	P-Forcing-D	.154±.004	.079±.008	.147±.001	.173±.002
	Original**	.071±.004	.011±.002	.045±.001	.041±.002

Table 9: Irregular time series (50% dropped)

	Method	Sines	Stocks	Energy	MuJoCo
Discriminative Score	KoVAE (Ours)	**.030±.017**	**.092±.075**	**.298±.013**	**.117±.019**
	GT-GAN	.372±.128	.265±.073	.317±.010	.270±.016
	TimeGAN-$\triangle t$	.496±.008	.487±.019	.479±.020	.483±.023
	RCGAN-$\triangle t$	.406±.165	.478±.049	.500±.000	.500±.000
	C-RNN-GAN-$\triangle t$	.500±.000	.500±.000	.500±.000	.500±.000
	T-Forcing -$\triangle t$	.408±.137	.308±.010	.478±.011	.486±.005
	P-Forcing-$\triangle t$	.428±.044	.388±.026	.498±.005	.491±.012
	TimeGAN-D	.500±.000	.477±.021	.473±.015	.500±.000
	RCGAN-D	.500±.000	.500±.000	.500±.000	.500±.000
	C-RNN-GAN-D	.500±.000	.500±.000	.500±.000	.500±.000
	T-Forcing-D	.430±.101	.407±.034	.376±.046	.498±.001
	P-Forcing-D	.499±.000	.500±.000	.500±.000	.500±.000
Predictive Score	KoVAE (Ours)	**.072±.002**	.019±.001	**.049±.001**	**.042±.001**
	GT-GAN	.101±.010	**.018±.002**	.064±.001	.056±.003
	TimeGAN-$\triangle t$	.123±.040	.058±.003	.501±.008	.402 ±.021
	RCGAN-$\triangle t$	.142±.005	.094±.013	.391±.014	.277±.061
	C-RNN-GAN-$\triangle t$	.741±.026	.089±.001	.500±.000	.448±.001
	T-Forcing-$\triangle t$	.379±.029	.075±.032	.251±.000	.069±.002
	P-Forcing-$\triangle t$	.120±.005	.067±.014	.263±.003	.189±.026
	TimeGAN-D	.169±.074	.254±.047	.339±.029	.375±.011
	RCGAN-D	.519±.046	.333±.044	.250±.010	.314±.023
	C-RNN-GAN-D	.754±.000	.273±.000	.438±.000	.479±.000
	T-Forcing-D	.104±.001	.038±.003	.090±.000	.113±.001
	P-Forcing-D	.190±.002	.089±.010	.198±.005	.207±.008
	Original	.071±.004	.011±.002	.045±.001	.041±.002

Table 10: Irregular time series (70% dropped)

|	Method	Sines	Stocks	Energy	MuJoCo
Discriminative Score	KoVAE (Ours)	**.065±.012**	**.101±.040**	**.392±.004**	**.119±.014**
	GT-GAN	.278±.022	.230±.053	**.325±.047**	.275±.023
	TimeGAN-$\triangle t$	.500±.000	.488±.009	.496±.008	.494±.009
	RCGAN-$\triangle t$	.433±.142	.381±.086	.500±.000	.500±.000
	C-RNN-GAN-$\triangle t$	.500±.000	.500±.000	.500±.000	.500±.000
	T-Forcing-$\triangle t$	.374±.087	.365±.027	.468±.008	.428±.022
	P-Forcing-$\triangle t$	.288±.047	.317±.019	.500±.000	.498±.003
	TimeGAN-D	.498±.006	.485±.022	.500±.000	.492±.009
	RCGAN-D	.500±.000	.500±.000	.500±.000	.500±.000
	C-RNN-GAN-D	.500±.000	.500±.000	.500±.000	.500±.000
	T-Forcing-D	.436±.067	.404±.068	.336±.032	.493±.005
	P-Forcing-D	.500±.000	.449±.150	.494±.011	.499±.000
Predictive Score	KoVAE (Ours)	**.076±.004**	**.012±.000**	**.052±.001**	**.044±.001**
	GT-GAN	.088±.005	.020±.005	.076±.001	.051±.001
	TimeGAN-$\triangle t$	.734±.000	.072±.000	.496±.000	.442±.000
	RCGAN-$\triangle t$	.218±.072	.155±.009	.498±.000	.222±.041
	C-RNN-GAN-$\triangle t$	.751±.014	.084±.002	.500±.000	.448±.001
	T-Forcing-$\triangle t$	.113±.001	.070±.022	.251±.000	.053±.002
	P-Forcing-$\triangle t$	.123±.004	.050±.002	.285±.006	.117±.034
	TimeGAN-D	.752±.001	.228±.000	.443±.000	.372±.089
	RCGAN-D	.404±.034	.441±.045	.349±.027	.420±.056
	C-RNN-GAN-D	.632±.001	.281±.019	.436±.000	.479±.001
	T-Forcing-D	.102±.001	.031±.002	.091±.000	.114±.003
	P-Forcing-D	.278±.045	.107±.009	.193±.006	.191±.005
	Original	.071±.004	.011±.002	.045±.001	.041±.002
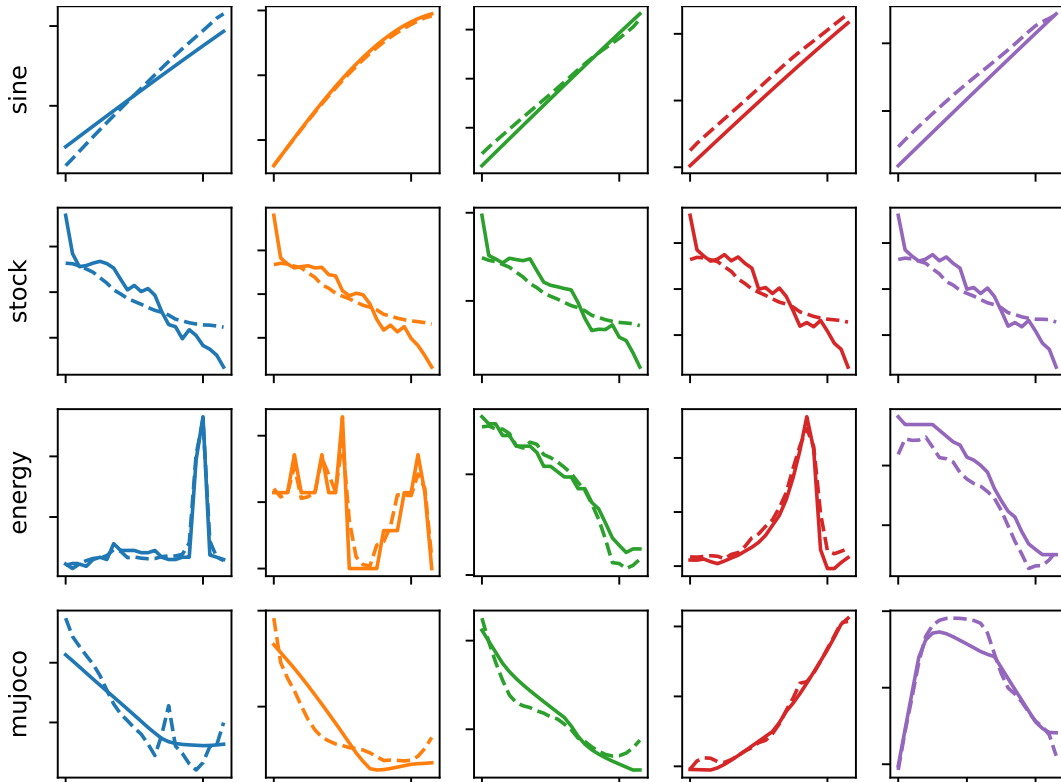
Figure 15: We plot the original signals (solid lines) vs. reconstructed signals (dashed lines) for Sine, Stock, Energy, and Mujoco in the regular setting. Overall, our model matches the data well.
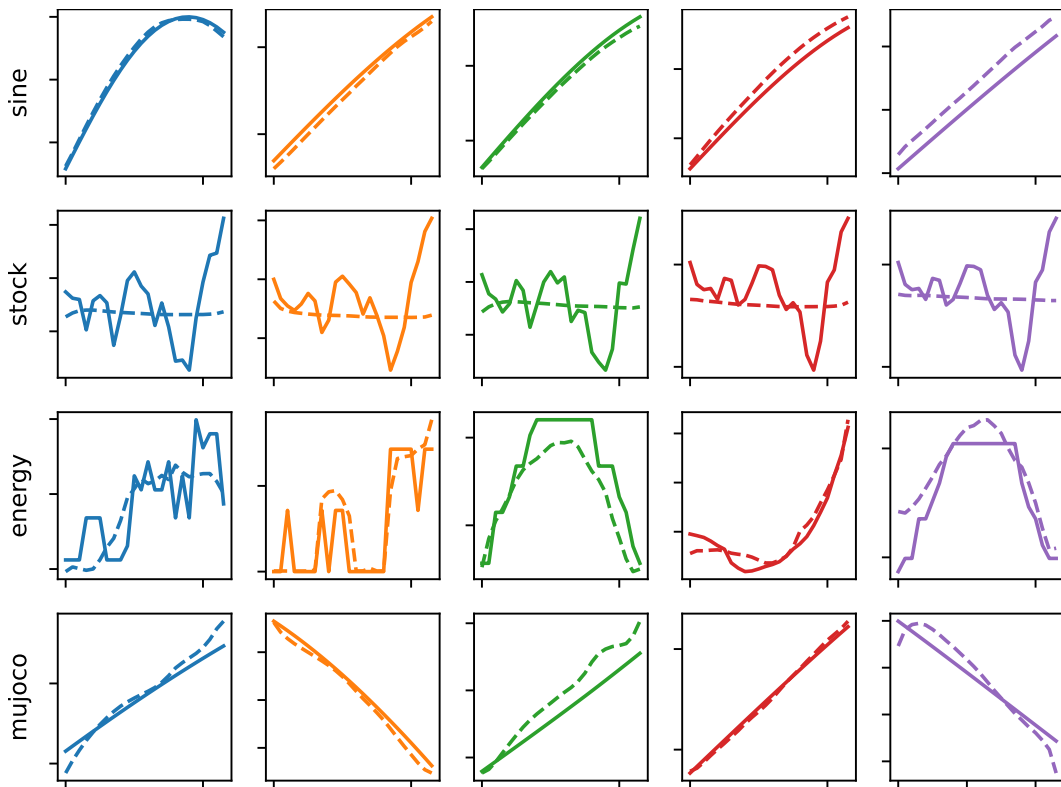
Figure 16: We plot the original signals (solid lines) vs. inferred signals (dashed lines) for Sine, Stock, Energy, and Mujoco in the irregular 50% case. Overall, our model recovers the data well, except for stock, where the output signal represents the average.